



**HAL**  
open science

## Infection-driven activation of transglutaminase 2 boosts glucose uptake and hexosamine biosynthesis in epithelial cells.

Benoit Maffei, Marc Laverrière, Yongzheng Wu, Sébastien Triboulet, Stéphanie Perrinet, Magalie Duchateau, Mariette Matondo, Robert Hollis, Charlie Gourley, Jan Rupp, et al.

### ► To cite this version:

Benoit Maffei, Marc Laverrière, Yongzheng Wu, Sébastien Triboulet, Stéphanie Perrinet, et al.. Infection-driven activation of transglutaminase 2 boosts glucose uptake and hexosamine biosynthesis in epithelial cells.. *EMBO Journal*, 2020, 39 (8), pp.e102166. 10.15252/embj.2019102166 . pasteur-02543964v1

**HAL Id: pasteur-02543964**

**<https://pasteur.hal.science/pasteur-02543964v1>**

Submitted on 15 Apr 2020 (v1), last revised 12 Jun 2020 (v2)

**HAL** is a multi-disciplinary open access archive for the deposit and dissemination of scientific research documents, whether they are published or not. The documents may come from teaching and research institutions in France or abroad, or from public or private research centers.

L'archive ouverte pluridisciplinaire **HAL**, est destinée au dépôt et à la diffusion de documents scientifiques de niveau recherche, publiés ou non, émanant des établissements d'enseignement et de recherche français ou étrangers, des laboratoires publics ou privés.



Distributed under a Creative Commons Attribution - NonCommercial 4.0 International License

1  
2  
3  
4  
5  
6  
7  
8  
9  
10  
11  
12  
13  
14  
15  
16  
17  
18  
19  
20  
21  
22  
23  
24  
25  
26  
27  
28

**Infection-driven activation of transglutaminase 2  
boosts glucose uptake and hexosamine biosynthesis**

Benoit Maffei<sup>1,2</sup>, Marc Laverrière<sup>1</sup>, Yongzheng Wu<sup>1</sup>, Sébastien Triboulet<sup>1</sup>, Stéphanie Perrinet<sup>1</sup>, Magalie Duchateau<sup>3</sup>, Mariette Matondo<sup>3</sup>, Robert L. Hollis<sup>4</sup>, Charlie Gourley<sup>4</sup>, Jan Rupp<sup>5</sup>, Jeffrey W. Keillor<sup>6</sup> and Agathe Subtil<sup>1\*</sup>

<sup>1</sup> Unité de Biologie cellulaire de l'infection microbienne, Institut Pasteur, CNRS UMR3691, 75015 Paris, France

<sup>2</sup> Sorbonne Université, Collège Doctoral, F-75005 Paris, France

<sup>3</sup> Plateforme Protéomique, Unité de Spectrométrie de Masse pour la Biologie, USR 2000 CNRS, Institut Pasteur, Paris, France

<sup>4</sup> Nicola Murray Centre for Ovarian Cancer Research, Cancer Research UK Edinburgh Centre, MRC IGMM, University of Edinburgh, Edinburgh, UK

<sup>5</sup> Department of Infectious Diseases and Microbiology, University of Lübeck, Lübeck, Germany

<sup>6</sup> Department of Chemistry and Biomolecular Sciences, University of Ottawa, Canada

\* Corresponding author: Unité de Biologie cellulaire de l'infection microbienne  
25 rue du Dr Roux, 75015 Paris, France  
Tel: +33 1 40 61 30 49  
Fax: + 33 1 40 61 32 38  
E-mail: [asubtil@pasteur.fr](mailto:asubtil@pasteur.fr)

29 ABSTRACT

30  
31

32 Transglutaminase 2 (TG2) is a ubiquitous enzyme with transamidating activity. We  
33 report here that the expression and activity of TG2 are enhanced in cells infected with the  
34 obligate intracellular bacteria *Chlamydia trachomatis*. Genetic or pharmacological inhibition  
35 of TG2 activity impair bacterial development. We show that TG2 increases glucose import by  
36 up-regulating the transcription of the glucose transporter genes *GLUT-1* and *GLUT-3*.  
37 Furthermore, TG2 activation drives one specific glucose-dependent pathway in the host, i.e.  
38 hexosamine biosynthesis. Mechanistically, we identify the glucosamine:fructose-6-phosphate  
39 amidotransferase (GFPT) among the substrates of TG2. GFPT modification by TG2 increases  
40 its enzymatic activity, resulting in higher levels of UDP-N-acetylglucosamine biosynthesis. As  
41 a consequence, TG2 activation results in increased protein O-GlcNAcylation. The correlation  
42 between TG2 transamidating activity and O-GlcNAcylation is disrupted in infected cells  
43 because host hexosamine biosynthesis is being exploited by the bacteria, in particular to assist  
44 their division. In conclusion, our work establishes TG2 as a key player in controlling glucose-  
45 derived metabolic pathways in mammalian cells, themselves hijacked by *C. trachomatis* to  
46 sustain their own metabolic needs.

47  
48

49 KEYWORDS: Chlamydia / GFPT / Hexosamine biosynthesis / O-GlcNAcylation /  
50 Transglutaminase 2

51  
52

53 INTRODUCTION

54  
55 The enzyme transglutaminase 2 (TG2) is an extremely versatile protein exhibiting  
56 transamidase, protein disulfide isomerase and guanine and adenine nucleotide binding and  
57 hydrolyzing activities (Gundemir, Colak et al., 2012). Also designated as “tissue  
58 transglutaminase”, it is ubiquitously expressed in the cytoplasm and at the cell surface in  
59 association with the extracellular matrix (Eckert, Kaartinen et al., 2014). The transamidase  
60 activity is the best described activity, and it is regulated by  $Ca^{2+}$  (Folk, Mullooly et al., 1967). It  
61 results in the formation of cross-links between proteins, or of post-translational modification  
62 of a protein substrate through incorporation of a small primary amine, or deamidation of a  
63 glutamine into a glutamate. Under steady-state conditions, TG2 exists in a compact, inactive  
64 conformation. Increase in intracellular  $Ca^{2+}$  concentration (upon stress, cell activation, etc)  
65 causes a conformational change, and the enzyme becomes catalytically active as a  
66 transamidase. Studies of genetically engineered mouse models and/or inherited disorders  
67 have implicated TG2 in several pathological conditions (Iismaa, Mearns et al., 2009). In  
68 particular, increased TG2 expression and transamidation activity is a common feature of many  
69 inflammatory diseases and events (Eckert et al., 2014). Possibly linked to its increased  
70 expression in inflammatory processes, several lines of evidence suggest the involvement of  
71 TG2 during cancer development (Huang, Xu et al., 2015).

72 Surprisingly, while the association between TG2 activity and inflammatory situations has  
73 been studied in several normal and pathological situations (Di Sabatino, Vanoli et al., 2012,  
74 Huang et al., 2015, Ientile, Curro et al., 2015, Iismaa et al., 2009, Liu, Kellems et al., 2017), the  
75 implication of this enzyme in a very classical inflammatory process, e.g. the defense response  
76 of a tissue to the invasion by a microorganism, has remained very poorly investigated.  
77 *Chlamydia trachomatis* is the most common sexually transmitted bacterial pathogen, and it  
78 develops inside a vacuole in a human host cell, typically an epithelial cell of the genital tract  
79 (reviewed in (AbdelRahman & Belland, 2005)). This obligate intracellular bacterium depends  
80 on the host to supply several essential metabolites, and in particular glucose (Gehre, Gorgette  
81 et al., 2016, Stephens, Kalman et al., 1998). Epithelial cells respond to the infection with the  
82 secretion of proinflammatory cytokines such as interleukin-6 (IL-6) and IL-8 (Rasmussen,  
83 Eckmann et al., 1997). The inflammatory response is exacerbated upon reinfection, ultimately  
84 leading to tissue damage such as hydrosalpinx and fibrosis (Brunham & Rey-Ladino, 2005). In  
85 this work, we show that TG2 becomes activated during the infection of epithelial cells with *C.*  
86 *trachomatis*, and is required for optimal bacterial growth. The investigation of the  
87 consequence of TG2 activation on host metabolism and the identification of targets of TG2  
88 transamidase activity during infection uncovered the control exerted by this enzyme on  
89 glucose import and on the hexosamine biosynthesis pathway, two metabolic features that are  
90 exploited by *C. trachomatis*.

91  
92  
93

94 RESULTS

95

96 **TG2 is highly expressed and becomes active during *C. trachomatis* infection**

97 A widely-used technique to probe TG2 activation is to measure the incorporation of  
98 biotin pentylamine (BP) into proteins. When present in excess, this membrane permeable  
99 primary amine out-competes other substrates for the transamidase reaction catalyzed by TG2  
100 and becomes covalently linked to glutamine residues of TG2 substrate proteins. The biotin  
101 group is then easily detectable by western blot using streptavidin coupled to horseradish  
102 peroxidase (HRP) (Lee, Maxwell et al., 1992). This procedure was applied to HeLa cells infected  
103 or not for 48 h with *C. trachomatis*. In non-infected samples, BP incorporation was extremely  
104 low, as expected since in resting cells low  $Ca^{2+}$  concentration maintains TG2 in an inactive  
105 conformation (Gundemir et al., 2012). In contrast, infected cells showed a significant  
106 incorporation of BP. CP4d, an inhibitor of TG2 transamidating activity (Caron, Munsie et al.,  
107 2012), abolished BP incorporation in a dose-dependent manner, indicating that BP  
108 incorporation was the result of the transamidase activity of TG2 (Fig. 1A). Live proliferating  
109 bacteria were needed for TG2 activation since filtered or heat-inactivated bacteria, or bacteria  
110 treated with the antibiotic doxycycline immediately after infection to prevent their  
111 proliferation, failed to induce BP incorporation (Fig. 1B and Fig. S1). BP incorporation upon  
112 infection was also observed in wild type mouse embryonic fibroblasts (MEFs) but not in MEFs  
113 isolated from *tgm2* knocked-out animals (TG2<sup>-/-</sup>), further supporting the implication of TG2 in  
114 this process (Fig. 1C).

115 Probing cellular lysates using anti-TG2 antibodies showed that activation of TG2 was  
116 accompanied with an increased expression of the enzyme (Fig. 1D). Consistent with this  
117 observation, inhibition of protein synthesis with cycloheximide decreased infection-induced  
118 BP incorporation (Fig. 1B). Reverse transcription followed by quantitative PCR (RT-qPCR)  
119 measurements revealed a 3- to 4-fold increase in the *TGM2* gene transcripts in infected versus  
120 non-infected cells, demonstrating that the increase in TG2 amount during infection is at least  
121 partly controlled at the transcriptional level (Fig. 1E). Interestingly, a positive feedback loop  
122 controls in part TG2 expression since *TGM2* transcription was no longer enhanced by infection  
123 when cells were treated with CP4d (Fig. 1E). *TGM2* transcription responds to a number of  
124 external stimuli including retinoic acid, hypoxia, and inflammatory cytokines such as IL-6  
125 (Eckert et al., 2014, Suto, Ikura et al., 1993). We reasoned that IL-6 might be implicated in the  
126 transcriptional up-regulation of TG2 in *Chlamydia* infected cells as this cytokine is produced  
127 during infection (Rasmussen et al., 1997). We first verified that *TGM2* transcription showed a  
128 dose-dependent response to the addition of recombinant IL-6 in the culture medium (Fig. 1F).  
129 To test if IL-6 contributes to the transcriptional up-regulation of *TGM2* during infection we  
130 next performed the infection in the presence of anti-IL-6 receptor antibodies. We observed a  
131 reduction of *TGM2* transcription in infected cells with increasing concentrations of antibodies  
132 in the culture medium (Fig. 1G). Altogether, these data indicate that the induction of *TGM2*  
133 transcription in *C. trachomatis* infected cells is at least in part a consequence of IL-6 secretion  
134 in response to infection, followed by signaling through the IL-6 receptor.

135 In conclusion, *C. trachomatis* infection increases TG2 levels and activates its  
136 transamidase activity.

137

### 138 **TG2 activity sustains bacterial growth**

139 To determine if TG2 activity affected bacterial development, we infected HeLa cells in  
140 the presence or not of the transamidase inhibitor CP4d. Thirty hours later, the progeny was  
141 collected and the number of infectious bacteria was determined by infecting fresh cells.  
142 Inhibition of TG2 activity with 40  $\mu$ M CP4d resulted in a 2-fold decrease in bacterial progeny  
143 (Fig. 2A). Consistently, a similar reduction in bacterial progeny was observed when TG2 activity  
144 was inhibited by cysteamine, another less specific inhibitor of TG2 (Figure EV1A). Progeny was  
145 also reduced when the bacteria were grown on TG2<sup>-/-</sup> MEFs compared to TG2<sup>+/+</sup>, indicating  
146 that the effect we had observed with TG2 inhibitors was not due to a direct toxicity of CP4d  
147 or cysteamine on the bacteria (Fig. EV1B). Consistent with these observations, silencing TG2  
148 expression with two different siRNA resulted in up to a 3-fold decrease in progeny (Fig. 2B).  
149 To confirm these findings in primary cells, we used epithelial cells isolated from fallopian tubes  
150 (Roth, Konig et al., 2010). CP4d was even more potent at reducing the progeny after one  
151 developmental cycle in these cells than in HeLa cells, as a ten-fold reduction was observed for  
152 10  $\mu$ M CP4d (Fig. 2C). The negative impact of TG2 inhibition on bacterial development was  
153 also observed in primary cells infected with *C. trachomatis* serovar D, showing that the effect  
154 is not restricted to the LGV biovar (Fig. 2C).

155 Reduced progeny could result from impairment of one or several of the steps of the  
156 chlamydial developmental cycle: adhesion, entry, differentiation into the replicative form,  
157 proliferation, and differentiation into the infectious form. We observed that the absence of  
158 TG2 in TG2<sup>-/-</sup> MEFs had no effect on bacterial adhesion (Fig. EV1C), but that it decreased the  
159 efficiency of bacterial internalization (Fig. EV1D). Consistently, 40  $\mu$ M CP4d decreased the  
160 percentage of infected cells by about 2-fold in HeLa cells (Fig. 2D). In addition, inclusions were  
161 smaller in cells treated with CP4d, and contained less bacteria, indicating that bacterial growth  
162 was slower in the absence of TG2 activity (Fig. 2D). The reduction of inclusion size when TG2  
163 was inhibited was also observed in primary cells infected with *C. trachomatis* L2 or serovar D  
164 (Fig. 2E).

165 We next tested the incidence of the absence of TG2 on chlamydial development in a  
166 mouse model of infection. *Chlamydia muridarum* is a mouse-adapted strain genetically very  
167 close to *C. trachomatis* (Read, Brunham et al., 2000). Infection of HeLa cells with *C. muridarum*  
168 also activated TG2 (Fig. EV2A), and we observed the same effect of silencing TG2 on *C.*  
169 *muridarum* growth as on *C. trachomatis* (Fig. EV2B). We infected TG2<sup>+/+</sup> and TG2<sup>-/-</sup> mice  
170 intravaginally with *C. muridarum* and 25 days after infection, mice were sacrificed and the  
171 genital tract was isolated (Fig. 2F). DNA was extracted from the upper genital tract and  
172 bacterial load was determined by qPCR. A slightly higher number of mice retained detectable  
173 bacterial DNA in the wild type group (10/16, 62 %, for the TG2<sup>+/+</sup> and 4/9, 44% for the TG2<sup>-/-</sup>  
174 mice). Among the animals in which bacterial DNA was still detected, the trend was for a higher  
175 bacterial load in the wild type background, but the number of TG2<sup>-/-</sup> animals we could breed

176 was too low for statistical significance. These data indicate that the absence of TG2 reduces  
177 only marginally, if at all, the ability for *C. muridarum* to establish an infection. It is however  
178 possible that in some tissues the loss of TG2 is compensated by expression of other  
179 transglutaminases, limiting the interpretation of these data (Iismaa et al., 2009). One clear  
180 difference between the two groups came from anatomical observations: TG2<sup>-/-</sup> animals  
181 showed milder signs of inflammation than their wild type littermate, especially when the  
182 oviduct hydrosalpinx scores were compared. It thus appears that the presence of TG2  
183 exacerbates the tissue damage in this mouse model of infection, in line with the implication  
184 of TG2 in tissue fibrosis (Eckert et al., 2014, Iismaa et al., 2009).

185

### 186 **TG2 plays a central role in metabolic rewiring**

187 We have recently shown that *C. trachomatis* acts as a glucose sink (Gehre et al., 2016).  
188 The host cell responds to glucose demand by increasing glucose uptake through  
189 overexpression of plasma membrane glucose transporters (Ojcius, Degani et al., 1998, Wang,  
190 Hybiske et al., 2017). Since we observed that TG2 level was increased during *C. trachomatis*  
191 infection, we wondered if this increase could control the concomitant increase in glucose  
192 transporter expression, as it does in mammary epithelial cells (Kumar, Donti et al., 2014). If  
193 this hypothesis was correct, one prediction that we could make was that low glucose  
194 availability in the culture medium should be more detrimental to bacterial growth in TG2<sup>-/-</sup>  
195 MEFs compared to the wild type MEFs, as TG2<sup>-/-</sup> MEFs would be impaired in their ability to  
196 adjust their glucose uptake to sustain bacterial growth. To test this hypothesis, we grew MEFs  
197 in medium containing decreasing concentrations of glucose and measured the number of  
198 infectious bacteria collected 30 hpi. As expected we observed that decreasing glucose  
199 availability resulted in a sharp decrease in bacterial titers, in both cellular backgrounds.  
200 However, bacterial titers were more sensitive to glucose deprivation in the TG2<sup>-/-</sup> MEFs than  
201 in the wild-type cells (Fig. 3A). For instance, at 1 mg/mL glucose, the progeny was reduced by  
202 82% in the TG2<sup>-/-</sup> MEFs, compared to only 35% in the TG2<sup>+/+</sup> MEFs.

203 To test the implication of TG2 in the rewiring of host metabolism more directly, we  
204 measured the incidence of TG2 inactivation on the cell capacity to uptake glucose. HeLa cells  
205 infected with *C. trachomatis* show increased transcription of *GLUT-1* and *GLUT-3*, which allows  
206 to increase glucose uptake and meet bacterial needs (Wang et al., 2017). We reproduced this  
207 result in HeLa cells, as well as in primary cells isolated from the endocervix (Fig. 3B). In  
208 contrast, in the presence of the TG2 inhibitor CP4d, the transcription of the glucose  
209 transporter genes was no longer induced by infection, indicating that TG2 is necessary for the  
210 control of *GLUT-1* and *GLUT-3* transcription. Absence of increase in *GLUT-1* and *GLUT-3*  
211 transcripts 48 hpi in the presence of CP4d was not due to the lower bacterial burden because  
212 when bacterial proliferation was interrupted 24 hpi by addition of doxycycline we observed a  
213 comparable reduction in bacterial load at 48 hpi as in cells treated with CP4d, but the  
214 transcription of the glucose transporter genes remained as high as in non-treated cells (Fig.  
215 S2).

216 Finally, to explore further the incidence of TG2 expression on that of glucose  
217 transporters we examined transcriptional data from a cohort of high grade serous ovarian  
218 cancer (HGSOC) patients. This population was chosen because clinical and biological data  
219 indicate that TG2 overexpression is an adverse prognostic factor in ovarian carcinoma (Hwang,  
220 Mangala et al., 2008, Shao, Cao et al., 2009). We observed a significant correlation between  
221 expression of *TGM2* and *GLUT-3* across the 265 clinical HGSOC specimens ( $\rho=0.50$ ,  $P<0.001$ )  
222 (Fig.3C). The HGSOC cohort also demonstrated significant correlation between TG2 and GLUT-  
223 1 expression, though the magnitude of correlation was less marked ( $\rho=0.21$ ,  $P<0.001$ ) (Fig.  
224 3C). Collectively, these data support the notion that TG2 plays a central role in regulating  
225 glucose transporters expression regulation in the context of infection or malignancy, thereby  
226 playing a central role in the control of the metabolic balance.

227

### 228 **The hypoxia-inducible factor 1 and the transamidase activity of TG2 are required for** 229 **the transcriptional up-regulation of glucose transporters**

230 One major transcriptional regulator of the expression of glucose transporters is the  
231 hypoxia-inducible factor 1 (HIF-1), which is increased during *Chlamydia* infection (Sharma,  
232 Machuy et al., 2011). Infection did not result in an increase in HIF-1 $\alpha$  transcripts, indicating  
233 that the increase in HIF-1  $\alpha$  occurs by stabilization of the transcription factor (Fig. 3D). To test  
234 whether HIF-1 was implicated in infection-induced up-regulation of glucose transport we  
235 silenced HIF-1 $\alpha$  expression before infecting the cells. Under these conditions, we observed a  
236 loss of induction of *GLUT-1* and *GLUT-3* transcription in infected cells. In contrast, the increase  
237 in *TGM2* transcripts upon infection remained, placing HIF-1 $\alpha$  downstream of *TGM2* induction  
238 (Fig. 3E).

239 In the presence of the TG2 inhibitor CP4d, the transcription of the glucose transporter  
240 genes was no longer induced by infection (Fig. 3B), indicating that the transamidase activity  
241 of TG2 was required. However, this observation could also be accounted for by the inhibition  
242 that CP4d exerts on TG2 expression in infection (Fig. 1E). To address directly the role of TG2  
243 transamidase activity in the regulation of the expression of glucose transporter genes we used  
244 TG2<sup>-/-</sup> MEFS in which TG2 wild-type or mutated for the transamidase activity (C277S mutant)  
245 were constitutively expressed (Rossin, D'Eletto et al., 2012). We focused on the regulation of  
246 *GLUT-1*, as we did not observe an increase in *GLUT-3* expression upon infection in this cellular  
247 background. Consistently with our previous findings, infection failed to induce an increase in  
248 *GLUT-1* transcripts in TG2<sup>-/-</sup> MEFS (Fig. 3F). Constitutive expression of wild-type TG2, but not  
249 of the C277S mutant, restored the induction of *GLUT-1* transcription upon infection. This  
250 observation demonstrates that the transamidase activity of TG2 is required for the increase  
251 in *GLUT-1* transcription upon infection.

252 Altogether, these data show that the transcription factor HIF-1, and TG2 transamidating  
253 activity, are both required for the up-regulation of glucose transporters during *C. trachomatis*  
254 infection.

255

### 256 **TG2 targets glutamine:fructose-6-P amidotransferase and enhances its activity**



257 In addition to its role in the up-regulation of the transcription of glucose transporter  
258 genes, TG2 may confer other benefits to *C. trachomatis*. To identify TG2 targets in the  
259 infectious process, HeLa cells were infected in the presence or absence of BP. Forty-eight  
260 hours later the cells were lysed and biotinylated proteins were isolated on streptavidin-coated  
261 beads, and identified by mass-spectrometry. Sixty-two proteins were found to be significantly  
262 enriched in the infected cell lysates grown in the presence of BP (Table S1). Fibronectin,  
263 galectin 3, RhoA, 40S ribosomal protein SA, immunoglobulin  $\kappa$  chain C region and hemoglobin  
264 beta were already identified as TG2 substrates (Guilluy, Rolli-Derkinderen et al., 2007, Mehul,  
265 Bawumia et al., 1995, Nelea, Nakano et al., 2008, Orrù, Caputo et al., 2003, Pincus & Waelsch,  
266 1968, Sohn, Chae et al., 2010). BAG2 and several other mitochondrial proteins were also  
267 enriched in the samples prepared in the presence of BP, in agreement with TG2 being present  
268 and active in this compartment (Altuntas, Rossin et al., 2015).

269 Among the potential TG2 substrates we identified in *C. trachomatis* infected cells, the  
270 enzyme glutamine:fructose-6-P amidotransferase (GFPT) caught our attention because it uses  
271 fructose-6-P as a substrate, which is derived from glucose-6-P. Moreover, both isoforms of  
272 the enzyme, GFPT1 (also called GFAT) and GFPT2, had been recovered from the proteomic  
273 approach, making it a very strong hit. We first confirmed that GFPT was recovered in the  
274 biotinylated fraction of cells infected with *C. trachomatis* in the presence of BP using anti-  
275 GFPT antibodies. The abundance of GFPT in the biotinylated fraction strongly decreased when  
276 infection had been performed in the presence of the TG2 inhibitor CP4d, demonstrating that  
277 incorporation of the biotinylated probe in GFPT depended on the activity of TG2 (Fig. 4A).

278 To further validate that GFPT is a novel substrate of TG2, purified TG2 and recombinant  
279 human GFPT1 (rhGFPT1) were incubated for 3 h at 37 °C in the presence of BP as primary  
280 amine donor. The incorporation of the biotinylated probe was analyzed by blotting with HRP-  
281 coupled streptavidin. The biotinylated probe was incorporated into rhGFPT1 in the presence  
282 and not in the absence of TG2. Furthermore, chelation of  $\text{Ca}^{2+}$  by EGTA inhibited the  
283 incorporation of the probe, as expected for a reaction dependent on the transamidase activity  
284 of TG2 (Fig. 4B). We concluded from these experiments that GFPT is a novel substrate of TG2  
285 that becomes modified by the transamidase activity of the enzyme during *C. trachomatis*  
286 infection.

287 In order to determine which glutamine residue(s) of GFPT1 was modified by TG2 *in*  
288 *vitro*, we analyzed the products of the reaction by mass spectrometry. BP incorporation was  
289 identified in ten glutamine residues (out of twenty-eight, Fig. 4C), presumably because  
290 promiscuous reactions occur *in vitro*. Among those, two glutamine residues were identified as  
291 prone to modification by TG2 using bioinformatics tools designed to score the peptidic  
292 environment favorable for TG2 activity, namely Q328 and Q555 (Keresztessy, Csoz et al.,  
293 2006, Sugimura, Hosono et al., 2006). We thus generated a glutamine to asparagine point  
294 mutant for each of these residues to minimize the impact on protein folding. As a control, we  
295 also mutated Q58, another candidate target identified by mass spectrometry but not  
296 surrounded by a consensus sequence for TG2. Purified recombinant proteins were incubated  
297 with TG2 and BP for 30 min at 37 °C before stopping the reaction. BP incorporation was

298 significantly reduced only in the rhGFPT1 Q328N, indicating that the Q328 is a prominent  
299 glutamine for modification by TG2 (Fig. 4D).

300 The fact that *C. trachomatis* produce their own GFPT (named GImS) prevented us from  
301 measuring the consequence of TG2 activation on host GFPT activity in infected cells. However,  
302 ionomycin is a widely used TG2 activator, as this Ca<sup>2+</sup> ionophore increases intracellular Ca<sup>2+</sup>  
303 concentration, which opens TG2 in its active conformation. We thus measured GFPT activity  
304 in lysates of cells treated or not with ionomycin, and analyzed the reaction products by high  
305 performance anion exchange chromatography (Fig. S3). We observed a three-fold increase in  
306 GFPT activity in cells treated with ionomycin, indicating that GFPT modification by TG2  
307 increases the activity of the enzyme (Fig. 4E).

308

### 309 **Modification of GFPT by TG2 enhances the hexosamine biosynthesis pathway**

310 The reaction catalyzed by GFPT is the first and rate limiting step of the hexosamine  
311 biosynthesis pathway (HBP, Fig. 5A). The HBP leads to the formation of uridine 5'-diphospho-  
312 *N*-acetylglucosamine (UDP-GlcNAc), which is further used for *N*-glycosylation, *N*-glycan  
313 branching, and *O*-linked *N*-acetylglycosylation (*O*-GlcNAcylation) in the ER, Golgi, and  
314 nucleus/cytosol, respectively. *O*-GlcNAcylation involves the transfer of a single UDP-GlcNAc  
315 moiety to the hydroxyl groups of serine or threonine residues. Two enzymes, *O*-  
316 GlcNAc transferase (OGT) and *O*-GlcNAcase (OGA), catalyze *O*-GlcNAc addition and removal,  
317 respectively and the *O*-GlcNAc modification level of proteins is directly dependent on the  
318 concentration of UDP-GlcNAc, the donor substrate for OGT (Kreppel & Hart, 1999). To confirm  
319 that GFPT modification by TG2 increased its activity and thus hexosamine biosynthesis we  
320 measured the level of *O*-GlcNAcylation in primary epithelial cells. We observed an increase in  
321 *O*-GlcNAcylation in cells treated with ionomycin. This increase was dependent on TG2 activity  
322 since it was not observed in the presence of the TG2 inhibitor CP4d (Fig. 5B) or in cells in which  
323 *TGM2* expression had been silenced using siRNA (Fig. 5C). Altogether these experiments show  
324 that activation of TG2 transamidase activity enhances the HBP.

325

### 326 **The increase in the hexosamine biosynthetic pathway is hijacked by the bacteria**

327 Surprisingly, we did not observe an increase in *O*-GlcNAcylation in cells infected for 48  
328 h by *C. trachomatis* (Fig. 6A). Since *O*-GlcNAcylation directly depends on UDP-GlcNAc  
329 concentration this observation suggests that UDP-GlcNAc levels in the cytoplasm are not  
330 significantly increased in infected cells. We have previously demonstrated that *C. trachomatis*  
331 co-opts SLC35D2, a host antiporter transporting UDP-GlcNAc, UDP-glucose and GDP-mannose  
332 to import these metabolites into the vacuole in which the bacteria develop (Gehre et al.,  
333 2016). We reasoned that UDP-GlcNAc might not accumulate in the cytoplasm in infected cells  
334 because it was relocated to the inclusion lumen. Supporting this hypothesis, we observed that  
335 activation of TG2 by ionomycin elicited a lower increase in *O*-GlcNAcylation in infected cells  
336 compared to non-infected cells, indicating that less free UDP-GlcNAc is available for *O*-  
337 GlcNAcylation in the infected host cytoplasm (Fig. 6B). Importantly GFPT expression was

338 stable in all conditions, indicating that the decrease in *O*-GlcNAcylation in infected cells is not  
339 due to lower GFPT expression (Fig. 6A-B).

340 In Gram-negative bacteria, UDP-GlcNAc supply is mostly used for lipopolysaccharide and  
341 peptidoglycan biosynthesis. *C. trachomatis* do not have a classical cell wall but use  
342 peptidoglycan synthesis for bacterial division (Liechti, Kuru et al., 2016). If UDP-GlcNAc, or an  
343 intermediate along the hexosamine biosynthesis pathway, was consumed at least partly in  
344 making bacterial peptidoglycan, lowering hexosamine biosynthesis should delay bacterial  
345 division, resulting in larger bacteria being formed. We tested this hypothesis by measuring the  
346 consequence of silencing GFPT, the rate-limiting enzyme in hexosamine biosynthesis, on  
347 bacterial size. The mass spectrometry data showed that both isoforms GFPT1 and GFPT2 were  
348 expressed in HeLa cells (Table S1). Comparison of the efficiency of siRNA designed to target  
349 specifically one isoform showed that GFPT2 was hardly detectable and targeting GFPT1 was  
350 sufficient to strongly decrease GFPT expression (Fig. 6C). We thus lowered hexosamine  
351 biosynthesis by treating cells with a siRNA against GFPT1 prior to infection, fixed the cells at  
352 increasing time of infection and used flow cytometry to measure bacterial sizes. As expected,  
353 the number of replicative bacteria increased with infection time (Fig. S4). Furthermore, it was  
354 recently demonstrated that replicative bacteria gradually decrease in size over the course of  
355 the developmental cycle (Lee, Enciso et al., 2017). We indeed observed a decrease in bacterial  
356 diameter over a 20 to 26 hpi time course, thereby validating the use of flow cytometry to  
357 measure the size of *C. trachomatis* (Fig. S4 and 6D). In cells treated with a siRNA against GFPT1  
358 the mean bacterial diameter became significantly higher than in control cells 24 hpi (Fig. 6D).  
359 We confirmed this result by measuring the diameter of bacteria on electron microscopy  
360 pictures of cells infected for 30 h (Fig. EV3). These kinetics fit well with our observation that  
361 TG2 activity increases between 24 and 48 hpi, when bacterial load is high, and access to  
362 nutrients might become limiting (Rother, Gonzalez et al., 2018). These observations support  
363 the hypothesis that a product of the hexosamine biosynthesis pathway is captured by the  
364 inclusion to support division. Consistent with a role for GFPT activity in sustaining bacterial  
365 growth we observed a reduction in the number of bacteria per inclusion 24 h post infection in  
366 the cells treated with siRNA against GFPT1, and the progeny collected was reduced 3-fold (Fig.  
367 6E). Of note, silencing of GFPT1 had no incidence on bacterial entry and the initiation of  
368 bacterial development, as the percentage of infected cells was identical to that in control cells  
369 (Fig. 6E). Altogether, these data strongly support the hypothesis that the increase in  
370 hexosamine biosynthesis by the host upon GFPT modification by TG2 is exploited by the  
371 bacteria, in particular to assist bacterial division. Interestingly, we observed that silencing TG2  
372 also increased bacterial size (Fig. 6D). While silencing TG2 has multiple effects beyond  
373 harnessing the HBP, these data are fully consistent with GFPT activation being one of the  
374 major outcomes of TG2 upregulation during *C. trachomatis* infection.

375

376

377

## DISCUSSION

378

379 TG2 transamidase activity is very potent, and would be deleterious if not tightly  
380 controlled. In basal conditions it is mostly turned off, and it is thought that under specific stress  
381 conditions, the enzyme might be locally turned on and transamidate specific substrates. The  
382 infection with *C. trachomatis* provided a unique physiological situation where the expression  
383 and activity of the enzyme were increased over a relatively short period of time in a  
384 physiological set-up. We took advantage of this observation to identify TG2 substrates. Among  
385 the 62 candidates identified, we focused on the enzyme GFPT. We showed that GFPT  
386 modification by TG2 increased its activity, resulting in higher hexosamine biosynthesis, a  
387 process also fueled by the positive control exerted by TG2 on glucose transporters expression.  
388 The product of the HBP, UDP-GlcNAc, is used for post-translational modification of proteins  
389 by *O*-GlcNAcylation. Thus, our work uncovered an unsuspected link between TG2  
390 transamidase activity and *O*-GlcNAcylation. This link was disrupted in infected cells because  
391 the increase in hexosamine biosynthesis in the host was exploited by the bacteria, in particular  
392 to assist their division. In conclusion, our work establishes TG2 as a key player in controlling  
393 glucose-derived metabolic pathways in mammalian cells, themselves hijacked by *C.*  
394 *trachomatis* to sustain their own metabolic needs (Fig. 6F).

395 Several inflammatory conditions are associated with an increase in TG2 expression  
396 (Eckert et al., 2014). We confirmed that IL-6 up-regulates *TGM2* transcription (Eckert et al.,  
397 2014, Suto et al., 1993) and we showed that this cytokine is implicated in the increase in *TGM2*  
398 transcription during *C. trachomatis* infection (Rasmussen et al., 1997) since anti-IL-6 receptor  
399 antibodies antagonized the induction of TG2 expression. How the enzyme becomes activated  
400 is less clear. In the cell  $Ca^{2+}$  concentration is high in the endoplasmic reticulum, and this  
401 compartment is tightly associated to the inclusion membrane (Derré, Swiss et al., 2011). The  
402 unfolded protein response pathway is activated in infected cells (George, Omosun et al.,  
403 2016), a condition that might be sufficient to activate TG2 (Lee, Jeong et al., 2014). Indeed  
404 accumulation of cytoplasmic  $Ca^{2+}$  around the inclusion has been reported (Majeed, Krause et  
405 al., 1999), which might be enough to locally activate TG2.

406 Treatment of cells with a potent inhibitor of TG2, CP4d, reduced progeny ten-fold in  
407 primary epithelial cells (Fig. 2). We have shown that the inhibition of TG2 activity had two  
408 distinct effects on *C. trachomatis* developmental cycle. First, it reduced the ability for the  
409 bacteria to enter the cells (Fig. S2). *C. trachomatis* use multiple receptors and appear to hijack  
410 several entry pathways into epithelial cells (Ford, Nans et al., 2018). The positive role played  
411 by TG2 on bacterial entry, which could be exerted from its intracellular or extracellular  
412 location, remains to be studied in future work. One attractive candidate mechanism is PDGFR  
413 signaling, since it is implicated in *C. trachomatis* entry (Elwell, Ceesay et al., 2008) and it is  
414 sensitive to TG2 activity (Nurminskaya, Beazley et al., 2014). Second, the inclusion developed  
415 slower in CP4d-treated culture, indicating that TG2 is necessary for optimal bacterial growth.  
416 We discuss below the two mechanisms we uncovered that account for the link between TG2  
417 activation and bacterial development, and place TG2 as a key regulator of bacterial access to  
418 glucose and its derivative UDP-GlcNAc.

419 We have shown that TG2 is required for the increase in transcription of *GLUT-1* and  
420 *GLUT-3* in infection in HeLa cells and in primary epithelial cells (Fig. 2). Glucose is an essential  
421 metabolite for *C. trachomatis* development and preventing the transcription of *GLUT-1* and  
422 *GLUT-3* by siRNA led to a two-fold decrease in progeny in HeLa cells (Wang et al., 2017). This  
423 result shows that glucose import can become limiting for bacterial growth, and thus that the  
424 control exerted by TG2 on the expression of glucose transporters accounts, at least in part,  
425 for the need for this enzyme for optimal bacterial growth. This conclusion is supported by our  
426 observation that glucose becomes limiting faster for bacterial progeny in MEFs lacking TG2  
427 than in wild-type cells. Thus, our study places TG2 as a key regulator for glucose import in  
428 infected cells.

429 Mechanistically, we showed that HIF-1 was required for *Chlamydia*-induced increase in  
430 the transcription of glucose transporters. HIF-1 $\alpha$  transcription does not increase during  
431 infection. TG2 interacts with HIF-1 $\beta$  (Filiano, Bailey et al., 2008), and an increase in TG2 levels  
432 upon infection might be sufficient to stabilize the HIF-1 complex. It is however not sufficient  
433 to account for infection-induced up-regulation of glucose transporters since we demonstrated  
434 that the transamidating activity of TG2 was required in this context. Through a series of  
435 elegant experiments the Johnson lab showed that the effect of TG2 on transcription was highly  
436 cell and context dependent (Gundemir, Colak et al., 2013, Gundemir, Monteagudo et al.,  
437 2017). TG2 modifies several transcription factors (Gundemir et al., 2012), but none of these  
438 known targets were recovered in our proteomic approach for the identification of TG2 targets  
439 upon infection. Furthermore, it was shown very recently that TG2 enhanced chromatin  
440 binding of the general transcription factor complex TFIID through the serotonylation of  
441 histone 3 trimethylated lysine 4 (Farrelly, Thompson et al., 2019). This, or another  
442 transglutaminase-mediated histone modification, might be implicated in the transcriptional  
443 control of glucose transporter genes in the infectious context.

444 Our proteomic approach identified 62 candidate TG2 substrates in *C. trachomatis*  
445 infection. Six of those were already known substrates of TG2, validating our analysis. We  
446 further demonstrated that GFPT was a substrate of TG2 and identified Q328 as a prominent  
447 transamidation site. The absence of shift in the migration profile of GFPT suggests that the  
448 amine donor is either a small protein, or a small amine, or that deamidation occurs, making  
449 identification by mass spectrometry very challenging. Experiments on GFPT  
450 immunoprecipitated from ionomycin-treated samples failed to detect histaminylation or  
451 serotonylation. Deamidation was occasionally seen on several glutamine residues, including  
452 Q328, raising questions as to the relevance of this observation that will be addressed in future  
453 studies.

454 We showed that GFPT activity was enhanced upon transamidation by TG2. This resulted  
455 in an increase in *O*-GlcNAcylation, since this post-translational modification of proteins is  
456 directly dependent on the concentration of UDP-GlcNAc (Kreppel & Hart, 1999). GFPT acts as  
457 a tetramer and is negatively regulated by several post-translational modifications (Chang, Su  
458 et al., 2000, Zibrova, Vandermoere et al., 2017) and by UDP-GlcNAc (Assrir, Richez et al., 2014).

459 Transamidation on Gln328 could interfere with these down-regulation mechanisms and  
460 thereby unleash the HBP.

461 Interestingly the positive correlation between TG2 activation and *O*-GlcNAcylation does  
462 not hold true in infected cells and our data indicate that this is due to hexosamines being  
463 consumed by the infection. Our observation that silencing GFPT expression increases bacterial  
464 diameter strongly supports the hypothesis that UDP-GlcNAc, or an intermediate along the  
465 HBP, is hijacked into the inclusion to fuel bacterial division, possibly by feeding peptidoglycan  
466 synthesis. Interestingly, a proximity-based labeling assay recently described an enrichment of  
467 TG2 and GFPT1 around the inclusion, suggesting that TG2 activation and GFPT modification  
468 might be most efficient in proximity of the bacteria-containing compartment (Olson, Widner  
469 et al., 2019). One recent publication showed that UDP-GlcNAc is also used during infection to  
470 post-translationally modify the intermediate filament vimentin and this also could contribute  
471 to significant UDP-GlcNAc consumption in *C. trachomatis* infection (Tarbet, Dolat et al., 2018).

472 The role played by TG2 in viral or microbial infections is raising increasing interest. Like  
473 in the case of *C. trachomatis* infection, genetic or pharmacological inhibition of TG2 led to a  
474 marked reduction in *Mycobacterium tuberculosis* replicative capacity. However, the  
475 mechanism involved might be different, since the data suggest that reduced replication in  
476 macrophages lacking TG2 is due to the impairment of autophagy homeostasis (Palucci, Matic  
477 et al., 2017). *M. tuberculosis* relies largely on lipids and fatty acids as energy source, and  
478 glucose availability might not be limiting in this case (Russell, VanderVen et al., 2010). Still, up-  
479 regulation of glucose transporter was also described in a mouse model of *M. tuberculosis*  
480 infection (Shi, Salamon et al., 2015), thus the involvement of TG2 in metabolism regulation in  
481 this context remains to be investigated.

482 There are multiple examples of host manipulation by pathogens that shed light on  
483 fundamental cellular processes. Here our work revealed an unsuspected regulation of the HBP  
484 by TG2. This discovery has important implications. Like other post-translational modifications,  
485 protein *O*-GlcNAcylation dramatically alters the fate and function of target proteins. In  
486 particular transcription factors are modified by *O*-GlcNAcylation, which implicates this  
487 modification in transcriptional regulation (Jackson & Tjian, 1988). Physiologically, disruption  
488 of *O*-GlcNAcylation homeostasis has been implicated in the pathogenesis of many human  
489 diseases, which include cancer, diabetes and neurodegeneration (Jóźwiak, Forma et al., 2014,  
490 Yang & Qian, 2017). The link between TG2 and *O*-GlcNAcylation means that TG2 activation is  
491 expected to have broad transcriptional consequences. In particular TG2 is activated in many  
492 cancers and future investigation is required to determine the contribution of the TG2/GFPT  
493 activation axis to tumorigenesis.

494

## 495 MATERIAL AND METHODS

496

### 497 **Cells and bacteria**

498

499 HeLa cells (ATCC) and mouse embryonic fibroblasts (MEFs) isolated from KO (TG2<sup>-/-</sup>) or WT  
500 (TG2<sup>+/+</sup>) C57B6 mice, were grown in Dulbecco's modified Eagle's medium with Glutamax

501 (DMEM, Invitrogen), supplemented with 10 % (v/v) heat-inactivated fetal bovine serum (FBS)  
502 (D'Eletto, Farrace et al., 2009). TG2<sup>-/-</sup> cells reconstituted with stable expression of wild type  
503 or C277S TG2 are described in (Rossin et al., 2012). Primary cells used for experiments  
504 displayed in Fig. 2 were isolated from human fallopian tubes and maintained in culture as  
505 previously described (Roth et al., 2010). Other primary cells were isolated from endocervix  
506 biopsies of female patients and were cultivated in keratinocyte-SFM medium (Thermo Fisher  
507 Scientific) containing 50 mg.L<sup>-1</sup> of bovine pituitary extract (Thermo Fisher Scientific) and 5 µg.L<sup>-1</sup>  
508 of epidermal growth factor (EGF) human recombinant (Thermo Fisher Scientific) (Wu *et al*,  
509 in preparation). All cell cultures were maintained at 37 °C, in 5 % CO<sub>2</sub> atmosphere and were  
510 routinely tested for mycoplasma using the standard PCR method. *C. trachomatis* serovar LGV  
511 L2 strain 434 and serovar D/UW-3/CX (ATCC), GFP-expressing L2 (L2<sup>incD</sup>GFP) or *C. muridarum*  
512 MoPn (for *in vivo* experiments) were propagated on HeLa cells, purified on density gradients  
513 as previously described and stored at -80 °C (Scidmore, 2005, Vromman, Laverriere et al.,  
514 2014).

515

#### 516 **siRNA treatment**

517

518 For siRNA experiments, 50 000 cells were plated in a 24-well plate and immediately mixed  
519 with Lipofectamine RNAiMAX (Invitrogen) following the manufacturer's recommendation,  
520 using 10 nM of siRNA (Table S2). For RB size assessment, 300 000 cells were plated in a 6-well  
521 plate. For electron microscopy experiments, 1.5 million cells were plated in a 25-cm<sup>2</sup> flask. For  
522 GFPT1 activity assay, 1 million cells were plated in a 10-cm diameter dish. The culture medium  
523 was changed the next day and experiments (infection or treatment with ionomycin) were  
524 performed two days post treatment with the siRNA.

525

#### 526 **GFPT1 purification**

527

528 Recombinant human GFPT1 (rhGFPT1) with an internal 6-His tag was produced from a plasmid  
529 pET28-rhGFPT1-6His in *E. coli* Rosetta (DE3) GlmS::Tc kindly given by Dr. Badet-Denisot  
530 (Centre de Recherche de Gif, France) (Li, Roux et al., 2007). The mutated form rhGFPT1 Q58N,  
531 rhGFPT1 Q328N and rhGFPT1 Q555N were obtained using QuikChange technology (Agilent)  
532 on the plasmid pET28-rhGFPT1-6His, with primers listed in Table S2, following the  
533 manufacturer instructions, and transformed in *E. coli* Rosetta (DE3) GlmS::Tc.

534 One litre of culture in 2YT medium supplemented with tetracycline (8 µg.mL<sup>-1</sup>, Sigma),  
535 kanamycin (50 µg.mL<sup>-1</sup>, Sigma), chloramphenicol (15 µg.mL<sup>-1</sup>, Sigma) and glucosamine  
536 (GlcNH<sub>2</sub>, 2 mg.mL<sup>-1</sup>, Sigma) was incubated with agitation at 37 °C until OD<sub>600</sub> reached 0.5.  
537 Protein expression was induced by addition of 0.5 mM of isopropyl β-D-thiogalactopyranoside  
538 (Sigma) at 25 °C for 24 h before being harvested. The cell pellets were resuspended in lysis  
539 buffer (16.27 mM Na<sub>2</sub>HPO<sub>4</sub> and 3.73 mM NaH<sub>2</sub>PO<sub>4</sub> pH 7.5, 200 mM NaCl, 20 mM imidazole,  
540 2 mM tris(2-carboxyethyl)phosphine hydrochloride (TCEP), 10 % glycerol, 1 mM fructose-6-P,  
541 Roche EDTA-free protease inhibitor cocktail) and disrupted by sonication. The recombinant  
542 protein was purified by incubation with Qiagen Ni-NTA agarose beads (Qiagen) for 1 h  
543 followed by three washing steps with the lysis buffer before elution with lysis buffer  
544 containing increasing concentrations of imidazole: 30 mM, 100 mM, 175 mM and finally 500  
545 mM of imidazole. The fractions containing the protein were dialyzed against lysis buffer with  
546 20 mM HEPES replacing the phosphate buffer before storage at -80 °C

547

#### 548 **TG2 activity assay**

549

550 *In vivo*: Cells plated the day before (100 000 cells/well) were infected with *C. trachomatis*  
551 serovar LGV L2 at a MOI of 1, and 0.5  $\mu$ M biotin pentylamine (BP) (Thermo Fisher Scientific)  
552 was added after 24 h. In some experiments, cells were pre-incubated for 2 h with 40  $\mu$ M CP4d  
553 or DMSO as control before addition of bacteria. CP4d inhibits the transamidase activity of TG2  
554 ( $K_i = 174$  nM) and favours its closed conformation (Caron et al., 2012). For experiments with  
555 ionomycin (Sigma), cells pre-treated with siRNA for 48 h or infected as described above for 24  
556 h were treated with Ionomycin and 0.5  $\mu$ M BP for 6 h.

557 At the end of the indicated incubation time, cells were lysed using 8 M urea buffer (30 mM  
558 Tris, 150 mM NaCl, 8 M urea, 1 % SDS, pH=8.0) and samples subjected to Western Blot.  
559

560 *In vitro*: 1 mU of transglutaminase from guinea pig liver (Sigma) was incubated at 37 °C for 15  
561 min or 3 h with 5  $\mu$ g of rhGFPT1, rhGFPT1 Q58N or rhGFPT1 Q328N and 1 mM of BP in 20 mM  
562 HEPES buffer pH 7.5, 200 mM NaCl, 2 mM TCEP, 10 % glycerol, 1 mM fructose-6-phosphate,  
563 10 mM CaCl<sub>2</sub>. The reaction was stopped by adding ethylene-bis(oxyethylenenitrilo)tetraacetic  
564 acid (EGTA) at a final concentration of 20 mM and boiling the samples 5 min at 95 °C.  
565

### 566 **Streptavidin-precipitation of TG2 targets**

567

568 Twenty million HeLa cells were seeded in a 163-cm<sup>2</sup> flask. One day later, the cells were  
569 infected or not with *C. trachomatis* serovar LGV L2 at a MOI = 1. Two hours post infection  
570 (hpi) the culture medium was changed and 40  $\mu$ M CP4d or DMSO was added. BP was added  
571 to the culture medium at 0.5 mM 24 h post treatment (infection or not) and cells were lysed  
572 46 hpi directly in the well using 8 M urea buffer. DNA was disrupted by sonication and a  
573 dialysis was performed against 2 M urea buffer (Tris 30 mM, NaCl 150 mM, 2 M urea, 1 % SDS,  
574 pH=8.0). Samples were incubated overnight at 4 °C with streptavidin-agarose beads (Sigma).  
575 After 3 washes with 2 M urea buffer and 3 washes with phosphate-buffered saline (PBS),  
576 proteins precipitated on the beads were eluted using Laemmli's buffer containing  
577 dithiothreitol (Sigma) boiled 5 min at 95 °C. Samples were then analyzed by Western blot or  
578 by mass spectrometry.  
579

### 580 **SDS-PAGE and Western blot**

581

582 Proteins were subjected to sodium dodecyl-sulfate polyacrylamide gel electrophoresis (SDS-  
583 PAGE) and transferred to a polyvinylidene difluoride (PVDF) membrane, which was blocked  
584 with 1 x PBS containing 5 % bovine serum albumin (BSA, for biotin revelation only) or milk and  
585 0.01 % Tween 20. The membranes were then immunoblotted with primary antibodies diluted  
586 in 1 x PBS containing 5 % milk and 0.01 % Tween 20. For analyzing the TG2 activity assay, biotin  
587 incorporation was revealed using streptavidin conjugated to HRP (#RPN1231, Sigma). Primary  
588 antibodies used in the western blots were the mouse clone 7D2 against TG2 (#ABIN1109303,  
589 Covalab), rabbit anti-serum against GFPT (kindly given by Dr. C. Weigert, University of  
590 Tübingen, Germany), mouse clone RL2 against O-GlcNAcylation (#MA1-072 Thermo Fisher  
591 Scientific) and mouse clone AC-74 against  $\beta$ -actin (#A5441 Sigma). Secondary antibodies were  
592 anti-mouse-HRP (#NA931, GE Healthcare) or anti-rabbit-HRP (#G-21234, Invitrogen)  
593 conjugated antibodies. Blots were developed using the Western Lightning  
594 Chemiluminescence Reagent (GE Healthcare).  
595

### 596 **Ovarian cancer cohort and statistical analysis**



597 Expression data for *TGM2*, *GLUT-1* and *GLUT-3* in 265 high grade serous ovarian cancers from  
598 Edinburgh were available from previous transcriptomic studies of ovarian cancer (Hollis,  
599 Churchman et al., 2019). Per-sample expression was calculated as the mean expression of  
600 probe-sets informative for each gene. Expression comparisons were performed using  
601 Spearman's rank correlation test. Spearman's rank correlation was chosen over Pearson's  
602 correlation following demonstration of non-normal expression distribution for TG2, GLUT-1  
603 and GLUT-3 (Shapiro-wilk normality test,  $P < 0.05$  for all).

604

## 605 **Mass Spectrometry**

606

607 *In solution protein digestion:* Samples were prepared in triplicate. For streptavidin-  
608 precipitation of TG2 targets samples, tryptic digestion was performed by enhanced filter-  
609 aided sample preparation. All steps were done in-filter. Briefly, samples were reduced (50 mM  
610 TCEP, 30 minutes at room temperature) and alkylated (50 mM iodoacetamide, 1 h at room  
611 temperature in the dark). Then, proteins were incubated overnight at 37 °C with 500bng  
612 trypsin (Trypsin Gold Mass Spectrometry Grade, Promega). Peptides were recovered by  
613 centrifugation.

614 After TG2/GFPT1 reactions *in vitro* samples were diluted in a large excess of 8 M urea / 100  
615 mM Tris HCl pH 8.5 buffer and then, as previously described, reduced (5 mM TCEP, 30 minutes  
616 at room temperature) and alkylated (10 mM iodoacetamide, 30 minutes at room temperature  
617 in the dark). Proteins were first digested for 5 h at 37 °C with 500 ng rLys-C Mass Spec Grade  
618 (Promega, Madison, WI, USA) before being diluted 4-fold with 100 mM Tris HCl pH 8.5 to reach  
619 a concentration below 2 M urea. Samples were then incubated overnight at 37 °C with 500 ng  
620 Sequencing Grade Modified Trypsin (Promega, Madison, WI, USA). To achieve the complete  
621 digestion of the peptides, a second incubation with the same amount of trypsin (5 h at 37 °C)  
622 was performed. Digestion was stopped by adding formic acid to 5 % final concentration and  
623 peptides were desalted and concentrated on Sep-Pak C<sub>18</sub>SPE cartridge (Waters, Milford, MA,  
624 USA) according to manufacturer instructions.

625

626 *Mass spectrometry analysis:* Tryptic peptides were analyzed on a Q Exactive Plus instrument  
627 (Thermo Fisher Scientific, Bremen) coupled with an EASY nLC 1 000 or 1 200 chromatography  
628 system (Thermo Fisher Scientific, Bremen). Sample was loaded on an in-house packed 50 cm  
629 nano-HPLC column (75 µm inner diameter) with C<sub>18</sub> resin (1.9 µm particles, 100 Å pore size,  
630 Reprosil-Pur Basic C<sub>18</sub>-HD resin, Dr. Maisch GmbH, Ammerbuch-Entringen, Germany) and  
631 equilibrated in 98 % solvent A (H<sub>2</sub>O, 0.1 % FA) and 2 % solvent B (ACN, 0.1 % FA). 120 or 180  
632 min gradient of solvent B at 250 nL.min<sup>-1</sup> flow rates were applied to separated peptides. The  
633 instrument method for the Q Exactive Plus was set up in DDA mode (Data Dependent  
634 Acquisition). After a survey scan in the Orbitrap (resolution 70 000), the 10 most intense  
635 precursor ions were selected for HCD fragmentation with a normalized collision energy set up  
636 to 28. Charge state screening was enabled, and precursors with unknown charge state or a  
637 charge state of 1 and > 7 were excluded. Dynamic exclusion was enabled for 35 or 45 seconds  
638 respectively.

639

640 *Data processing:* Data were searched using Andromeda with MaxQuant software 1.4.1.2 or  
641 1.5.3.8 version against respectively a *Chlamydia trachomatis* Uniprot reference proteome  
642 database concatenated with Homo sapiens Uniprot reference proteome database. Data were  
643 also searched against usual known mass spectrometry contaminants and reversed sequences  
644 of all entries or an *E. coli* K12 Uniprot reference proteome database concatenated with

645 rhGFPT1 and gpTGase proteins (Tyanova, Temu et al., 2016). Andromeda searches were  
646 performed choosing trypsin as specific enzyme with a maximum number of two missed  
647 cleavages. Possible modifications included carbamidomethylation (Cys, fixed), oxidation (Met,  
648 variable), N-ter acetylation (variable) and BP (Gln, variable). The mass tolerance in MS was set  
649 to 20 ppm for the first search then 6 ppm for the main search and 10 ppm for the MS/MS.  
650 Maximum peptide charge was set to seven and five amino acids were required as minimum  
651 peptide length. The “match between runs” feature was applied between replicates with a  
652 maximal retention time window of 2 or 0.7 min. One unique peptide to the protein group was  
653 required for the protein identification. A false discovery rate (FDR) cutoff of 1 % was applied  
654 at the peptide and protein levels.  
655

656 *Data analysis:* To validate the identification of the BP on the glutamine of modified peptides,  
657 spectra were manually inspected (or fragment assignments).

658 For the global quantification, output files from MaxQuant were used for protein  
659 quantification. Quantification was performed using the XIC-based LFQ algorithm with the Fast  
660 LFQ mode as described previously (Cox, Hein et al., 2014). Unique and razor peptides, included  
661 modified peptides, with at least 2 ratio count were accepted for quantification.

662 For pairwise comparisons, proteins identified in the reverse and contaminant databases and  
663 proteins only identified by site were first discarded from the list. Then, proteins exhibiting  
664 fewer than 2 LFQ values in at least one condition were discarded from the list to avoid  
665 misidentified proteins. After log<sub>2</sub> transformation of the leftover proteins, LFQ values were  
666 normalized by median centering within conditions (normalizeD function of the R package  
667 DAPAR (Wieczorek, Combes et al., 2017)). Remaining proteins without any LFQ value in one  
668 of both conditions have been considered as proteins quantitatively present in a condition and  
669 absent in another. They have therefore been set aside and considered as differentially  
670 abundant proteins. Next, missing values were imputed using the imp.norm function of the R  
671 package norm. Proteins with a foldchange under 2 have been considered not significantly  
672 differentially abundant. Statistical testing of the remaining proteins (having a foldchange over  
673 2) was conducted using a limma t-test thanks to the R package limma (Ritchie, Phipson et al.,  
674 2015). An adaptive Benjamini-Hochberg procedure was applied on the resulting p-values  
675 thanks to the function adjust.p of R package cp4p using the robust method of Pounds and  
676 Cheng to estimate the proportion of true null hypotheses among the set of statistical tests  
677 (Pounds & Cheng, 2006). The proteins associated to an adjusted p-value inferior to an FDR  
678 level of 1% have been considered as significantly differentially abundant proteins.  
679

## 680 **Adhesion assay**

681  
682 Adhesion assays were performed as described previously (Vromman et al., 2014). In brief,  
683 MEFs cells plated in 24-well plate the day before (100 000 cells/well) were pre-cooled 30 min  
684 at 4 °C and then were incubated for 4 h at 4 °C with L2<sup>Incd</sup>GFP bacteria at a MOI = 10, sonicated  
685 prior to infection in order to disrupt bacterial aggregates. Then cells were washed gently with  
686 PBS and detached using 0.5 mM EDTA in PBS. Samples were fixed 30 min in 2 % PFA, washed  
687 with PBS and analyzed using flow cytometry.  
688

## 689 **Bacterial entry assessment**

690  
691 Entry experiments were performed as described previously (Vromman et al., 2014). In brief,  
692 MEFs cells plated on coverslips in 24-well plate the day before (100 000 cells/well) were pre-

693 cooled 30 min at 4 °C and then incubated for 45 min at 4 °C with L2<sup>IncD</sup>GFP bacteria at a MOI  
694 = 10, sonicated prior to infection in order to disrupt bacterial aggregates. Then pre-warmed  
695 medium was added and coverslips were incubated at 37 °C before being fixed at different time  
696 points in 4 % PFA for 20 min. Extracellular bacteria were stained with a mouse anti-MOMP-  
697 LPS (Argene # 11-114) antibody followed with Cy5-conjugated anti-mouse (#PA45002,  
698 Amersham Biosciences) secondary antibody. The dilutions were made in PBS containing 3 %  
699 of BSA. DNA was stained using 0.5 µg.mL<sup>-1</sup> of Hoechst 33342 (Thermo Fisher Scientific) added  
700 in the secondary antibody solution. Images were acquired on an Axio observer Z1 microscope  
701 equipped with an ApoTomemodule (Zeiss, Germany) and a 63× Apochromat lens. Images were  
702 taken with an ORCAflash4.OLT camera (Hamamatsu, Japan) using the software Zen.

703

### 704 **Progeny assay**

705

706 For glucose privation tests on MEFs cells, 140 000 cells per well were seeded in a glucose-free  
707 DMEM (Invitrogen) supplemented with 10 % FBS. The following day, the medium was replaced  
708 with glucose-free DMEM supplemented with 10 % FBS and the indicated concentration of  
709 glucose (Sigma). The next day cells were infected with L2<sup>IncD</sup>GFP bacteria at a MOI = 0.2.

710 For progeny assays on HeLa cells, primary cells or MEFs cells, 100 000 cells were seeded in a  
711 24-well plate. The next day cells were pre-treated with CP4d (or DMSO) or cysteamine  
712 (Sigma #30078) (or water) for 2 h and infected with L2<sup>IncD</sup>GFP bacteria at a MOI = 0.15. Cells  
713 treated with siRNA for 48 h were directly infected with L2<sup>IncD</sup>GFP bacteria or *C. muridarum* at  
714 a MOI = 0.2. Thirty hpi, cells were detached and fixed in 2 % PFA in PBS prior to flow  
715 cytometry analysis in order to evaluate the first round of infection. In duplicate wells, cells  
716 were detached, lysed using glass beads and the supernatant was used to infect new  
717 untreated cells (or WT cells in the case of MEFs) plated the day before (100 000 cells/well in  
718 a 24-well plate), in serial dilution. The next day, 3 wells per condition with an infection lower  
719 than 30 % (checked by microscopy) were detached and fixed as described above, before  
720 analysis by flow cytometry and determination of the bacterial titer. In the case of *C.*  
721 *muridarum* infections, bacteria were stained after fixation with a rabbit anti-CmGroEL  
722 antibody followed with AlexaFluor488-conjugated anti-rabbit secondary antibody (A11034,  
723 Invitrogen). Dilutions were made in PBS containing 0.1 % of BSA and 0.05 % of saponin  
724 (Sigma). The anti-CmGroEL antibody was obtained by AgroBio (La Ferté Saint-Aubain) by  
725 immunizing one New Zeland white rabbit with *C. muridarum* GroEL prepared as described in  
726 (Illingworth, Ramsey et al., 2011). Acquisition was performed using a CytoFLEX S (Beckman  
727 Coulter) and 50 000 events per sample were acquired and then analyzed using FlowJo  
728 (version 10.0.7).

729

### 730 **Infection in mice**

731

732 Female TG2<sup>-/-</sup> and TG2<sup>+/+</sup> KO mice were kindly provided by Dr. C. Papista (INSERM UMR970,  
733 Centre de Recherche Cardiovasculaire, Paris) and maintained in the animal facility of the  
734 Institut Pasteur, Paris. All animals are treated with 2.5 mg of medroxyprogesterone (Depo-  
735 provera-SC®, Pfizer) 7 days prior to infection to synchronize the menstrual cycle. Mice were  
736 intravaginally inoculated with *C. muridarum*, 10<sup>5</sup> IFU per animal. Twenty-five days after  
737 infection, animals were sacrificed and the organs excised including cervix, uterine horn and  
738 oviduct. The bacterial burden in the excised organs, in the right part of the upper genital tract  
739 was measured by qPCR after DNA extraction using the DNeasy Blood and Tissue Kit (Qiagen).  
740 The left part of the upper genital tract was excised and rinsed into PBS for the morphological

741 observation. Hydrosalpinx score was determined as described (Peng, Lu et al., 2011).  
742 Procedures involving mice were previously approved by local Animal Ethics Committees and  
743 registered with the French authorities (APAFIS#8635-2017012314265571).

744

#### 745 **RT-qPCR and qPCR**

746

747 One hundred twenty-five thousand cells in a 24-well plate were infected or not with *C.*  
748 *trachomatis* serovar LGV L2 at a MOI = 1. Cells were treated with anti-IL-6 receptor antibody  
749 (Roactemra®, Roche) CP4d (40 µM) or DMSO 2 hpi, or doxycycline (62.5 ng.mL<sup>-1</sup>, Sigma) 24  
750 hpi. Cells pre-treated with siRNA for 48 h were directly infected with L2<sup>IncD</sup>GFP bacteria at a  
751 MOI = 1. For testing the response of HeLa cells to IL-6 treatment, 125 000 cells in 24-well plate  
752 were treated with recombinant human IL-6 (R&D Biosystems) for 18hrs.

753 Total RNAs were isolated 24 or 48 hpi with the RNeasy Mini Kit (Qiagen) with DNase treatment  
754 (DNase I, Roche). RNA concentrations were determined with a spectrophotometer NanoDrop  
755 (Thermo Fisher Scientific) and normalized to equal contents. Reverse transcription (RT) was  
756 performed using the M-MLV Reverse Transcriptase (Promega) and quantitative PCR (qPCR)  
757 undertaken on the complementary DNA (cDNA) with LightCycler 480 system using LightCycler  
758 480 SYBR Green Master I (Roche). For the experiments displayed in Fig. S2, a duplicate well  
759 was used to extract genomic DNA (gDNA) of each time point using the DNeasy Blood and  
760 Tissue Kit (Qiagen). Data were analyzed using the  $\Delta\Delta C_t$  method with the *actin* gene as a  
761 control gene (Schmittgen & Livak, 2008). Each RT-qPCR experiment was performed in  
762 duplicate and repeated at least three times.

763

#### 764 **GFPT activity assay**

765

766 HeLa cells treated with ionomycin (4 µM) or DMSO for 6 h were detached in lysis buffer  
767 containing 0.05 M Tris, 0.15 M NaCl, 5 % glycerol, 0.5% NP-4, protease inhibitor cocktail EDTA-  
768 free (Roche), pH 7.5. After lysis at 4 °C, NP-40 concentration was reduced by addition of an  
769 excess of reaction buffer (0.05 M Tris, 0.15 M NaCl, 5 % glycerol, protease inhibitor cocktail  
770 EDTA-free, pH 7.5) and cell debris were eliminated by centrifugation. Cell lysates were  
771 incubated 45 min at 37 °C with 0.6 mg.mL<sup>-1</sup> fructose-6-phosphate (Sigma) and 0.6 mg.mL<sup>-1</sup>  
772 glutamine (Sigma). The reaction was stopped by incubating the samples for 5 min at 100 °C  
773 and precipitates were removed by centrifugation. Analysis of the samples was performed by  
774 high performance anion exchange chromatography (HPAEC, Dionex, model ISC3000) on a  
775 CarboPAC-PA1 column (3.2 × 250 mm, Dionex) using 100 mM NaOH, and 720 mM NaOAc in  
776 100 mM NaOH, as eluent A and B, respectively. The column was pre-equilibrated for 20 min  
777 in 98 % A + 2 % B. Following sample injection, a gradient run (flow rate 1 mL.min<sup>-1</sup>) was  
778 performed as follows: 0–2 min, isocratic step (98 % A + 2 % B), 2–15 min 98 % A + 2 % B – 80  
779 % A + 20 % B, 15–20 min 80 % A + 20 % B – 57 % A + 43 % B, 20–22 min 57 % A + 43 % B – 100  
780 % B, and 22–25 min 100 % B. Samples were detected on a pulsed electrochemical detector.

781

#### 782 **Bacterial size measurement**

783

784 HeLa cells in a 6-well plate, treated with siRNA as described above, were infected every two  
785 hours with L2<sup>IncD</sup>GFP bacteria at a MOI = 0.3. The next day, all wells were detached and fixed  
786 simultaneously in 2 % PFA and 2.5 % glutaraldehyde (Sigma) in PBS. After 25 min, cells were  
787 broken using glass beads, vortexed and syringed (3 times, using 1 mL 26GA x 3/8-inch  
788 syringes). Samples were then analyzed by flow cytometry. An exponential culture of *E. coli*,

789 purified *C. trachomatis* elementary bodies (i.e. the infectious non-replicative form of the  
790 bacterium) and non-infected cells prepared the same way were used to gate successively for  
791 particles of equal size or smaller than *E. coli* (thereby excluding non-broken cells), larger than  
792 elementary bodies (thereby excluding non-dividing bacteria), and with positive green  
793 fluorescence (thereby excluding cell debris). The forward-scattered light (FSC-A) was used to  
794 compare bacterial diameters. Each data point represents the mean of at least 400 gated  
795 events.

796

### 797 **Electron microscopy**

798

799 One million five hundred thousand cells were transfected with siRNA and infected two days  
800 later. Cells were fixed 30 hpi with 2.5 % glutaraldehyde (v/v) (Electron Microscopy Sciences)  
801 in 0.1 M cacodylate buffer pH 7.4, for 1 h at room temperature. After several washes in  
802 cacodylate they were post-fixed with 1 % osmium tetroxide (w/v) in cacodylate for 1 h. After  
803 several washes with water the cells were progressively dehydrated with increasing  
804 concentrations of ethanol from 25 % to 100 %. The cells were then gradually embedded in  
805 epoxy resin. After overnight polymerization at 60 °C, 50 to 70 nm thin sections were cut in an  
806 ultra-microtome (Ultracut, Leica) and cells were imaged after post-staining with uranyl  
807 acetate and lead citrate in a T12-FEI transmission EM operated at 120kV.

808

809

### 810 DATA AVAILABILITY

811 The mass spectrometry proteomics data have been deposited to the ProteomeXchange  
812 Consortium via the PRIDE partner repository with the dataset identifier PXD017117.

813

### 814 ACKNOWLEDGEMENTS

815 We thank Anke Hellberg and Béatrice Niragire for technical assistance, Manuela D'Eletto for  
816 TG2<sup>-/-</sup> reconstituted MEFs, Dr Christina Papista for providing mice, Dr Denise Badet-Denisot  
817 for the rhGFPT1 plasmid and for advice, Dr Cora Weigert for anti-GFPT antibodies, Vishu  
818 Aimanianda Bopaiah for help with HPAEC, Dr Lingling Chen for CmGroEL, Augustin Latourte  
819 for Roactemra®. This work was supported by an ERC Starting Grant (NUChLEAR N°282046),  
820 the Institut Pasteur (GFP-LIMNEC METINF), the Centre National de la Recherche Scientifique  
821 and by GEFLUC. BM was funded by the Ministère de l'Éducation Nationale, de la Recherche et  
822 de la Technologie and by Cancéropole Ile-de-France.

823

824

### 825 AUTHOR CONTRIBUTIONS

826 AS, BM, ML and JWK conceived the study and designed the methodology. BM, ML, ST, SP  
827 conducted the experiments and performed data analysis and interpretation. YW conducted  
828 the experiments with mice and performed data analysis. MD and MM collected and analyzed  
829 the mass spectrometry data. RHL and CG collected and analyzed the HGSOc cohort data. JR  
830 collected and analyzed the infection data using cells isolated from the fallopian tube. JWK  
831 synthesized TG2 inhibitors. AS and BM wrote the original draft of the manuscript. MM, JWK  
832 edited the manuscript. AS and BM revised the manuscript. All authors commented on the  
833 manuscript. AS supervised the study and secured funding.

834

835 CONFLICT OF INTEREST

836 The authors declare that they have no conflict of interest.

837

838

839 REFERENCES

840

841 AbdelRahman YM, Belland RJ (2005) The chlamydial developmental cycle. *FEMS Microbiol Rev*  
842 29: 949-959

843 Altuntas S, Rossin F, Marsella C, D'Eleto M, Diaz-Hidalgo L, Farrace MG, Campanella M,  
844 Antonioli M, Fimia GM, Piacentini M (2015) The transglutaminase type 2 and pyruvate kinase  
845 isoenzyme M2 interplay in autophagy regulation. *Oncotarget* 6: 44941-44954

846 Assrir N, Richez C, Durand P, Guittet E, Badet B, Lescop E, Badet-Denisot MA (2014) Mapping  
847 the UDP-N-acetylglucosamine regulatory site of human glucosamine-6P synthase by  
848 saturation-transfer difference NMR and site-directed mutagenesis. *Biochimie* 97: 39-48

849 Brunham RC, Rey-Ladino J (2005) Immunology of Chlamydia infection: Implications for a  
850 Chlamydia trachomatis vaccine. *Nature Reviews Immunology* 5: 149-161

851 Caron NS, Munsie LN, Keillor JW, Truant R (2012) Using FLIM-FRET to Measure Conformational  
852 Changes of Transglutaminase Type 2 in Live Cells. *PLoS ONE* 7: e44159-7

853 Chang Q, Su K, Baker JR, Yang X, Paterson AJ, Kudlow JE (2000) Phosphorylation of human  
854 glutamine:fructose-6-phosphate amidotransferase by cAMP-dependent protein kinase at  
855 serine 205 blocks the enzyme activity. *J Biol Chem* 275: 21981-7

856 Cox J, Hein MY, Luber CA, Paron I, Nagaraj N, Mann M (2014) Accurate proteome-wide label-  
857 free quantification by delayed normalization and maximal peptide ratio extraction, termed  
858 MaxLFQ. *Molecular & cellular proteomics : MCP* 13: 2513-26

859 D'Eleto M, Farrace MG, Falasca L, Reali V, Oliverio S, Melino G, Griffin M, Fimia GM, Piacentini  
860 M (2009) Transglutaminase 2 is involved in autophagosome maturation. *Autophagy* 5: 1145-  
861 54

862 Derré I, Swiss R, Agaisse H (2011) The lipid transfer protein CERT interacts with the Chlamydia  
863 inclusion protein IncD and participates to ER-Chlamydia inclusion membrane contact sites.  
864 *PLoS Pathog* 7: e1002092

865 Di Sabatino A, Vanoli A, Giuffrida P, Luinetti O, Solcia E, Corazza GR (2012) The function of  
866 tissue transglutaminase in celiac disease. *Autoimmun Rev* 11: 746-53

867 Eckert RL, Kaartinen MT, Nurminskaya M, Belkin AM, Colak G, Johnson GVW, Mehta K (2014)  
868 Transglutaminase Regulation of Cell Function. *Physiol Rev* 94: 383-417

869 Elwell CA, Ceesay A, Kim JH, Kalman D, Engel JN (2008) RNA interference screen identifies Abl  
870 kinase and PDGFR signaling in *Chlamydia trachomatis* entry. *PLoS Pathog* 4: e1000021

871 Farrelly LA, Thompson RE, Zhao S, Lepack AE, Lyu Y, Bhanu NV, Zhang B, Loh Y-HE,  
872 Ramakrishnan A, Vadodaria KC, Heard KJ, Erikson G, Nakadai T, Bastle RM, Lukasak BJ, Zebroski  
873 H, Alenina N, Bader M, Berton O, Roeder RG et al. (2019) Histone serotonylation is a  
874 permissive modification that enhances TFIID binding to H3K4me3. *Nature* 567: 535-539

875 Filiano AJ, Bailey CD, Tucholski J, Gundemir S, Johnson GV (2008) Transglutaminase 2 protects  
876 against ischemic insult, interacts with HIF1beta, and attenuates HIF1 signaling. *FASEB J* 22:  
877 2662-75

878 Folk JE, Mullooly JP, Cole PW (1967) Mechanism of Action of Guinea Pig Liver  
879 Transglutaminase: II. THE ROLE OF METAL IN ENZYME ACTIVATION. *J Biol Chem* 242: 1838-  
880 1844

881 Ford C, Nans A, Boucrot E, Hayward RD (2018) Chlamydia exploits filopodial capture and a  
882 macropinocytosis-like pathway for host cell entry. *PLoS Pathog* 14: e1007051

883 Gehre L, Gorgette O, Perrinet S, Prevost MC, Ducatez M, Giebel AM, Nelson DE, Ball SG, Subtil  
884 A (2016) Sequestration of host metabolism by an intracellular pathogen. *Elife* 5: e12552

885 George Z, Omosun Y, Azenabor AA, Partin J, Joseph K, Ellerson D, He Q, Eko F, Bandea C,  
886 Svoboda P, Pohl J, Black CM, Igietseme JU (2016) The roles of unfolded protein response  
887 pathways in Chlamydiopathogenesis. *J Infect Dis*: jiw569

888 Guilluy C, Rolli-Derkinderen M, Tharaux P-L, Melino G, Pacaud P, Loirand G (2007)  
889 Transglutaminase-dependent RhoA Activation and Depletion by Serotonin in Vascular Smooth  
890 Muscle Cells. *J Biol Chem* 282: 2918-2928

891 Gundemir S, Colak G, Feola J, Blouin R, Johnson GV (2013) Transglutaminase 2 facilitates or  
892 ameliorates HIF signaling and ischemic cell death depending on its conformation and  
893 localization. *Biochim Biophys Acta* 1833: 1-10

894 Gundemir S, Colak G, Tucholski J, Johnson GV (2012) Transglutaminase 2: a molecular Swiss  
895 army knife. *Biochim Biophys Acta* 1823: 406-19

896 Gundemir S, Monteagudo A, Akbar A, Keillor JW, Johnson GVW (2017) The complex role of  
897 transglutaminase 2 in glioblastoma proliferation. *Neuro-oncology* 19: 208-218

898 Haneji T, Koide SS (1989) Transblot identification of biotin-containing proteins in rat liver. *Anal*  
899 *Biochem* 177: 57-61

900 Hollis RL, Churchman M, Michie CO, Rye T, Knight L, McCavigan A, Perren T, Williams A, G.  
901 MW, Kaplan RS, Jayson GC, Oza A, Harkin DP, Herrington CS, Kennedy R, Gourley C (2019) High  
902 EMSY expression defines a BRCA-like subgroup of high grade serous ovarian carcinoma with  
903 prolonged survival and hypersensitivity to platinum. *Cancer* 125: 2772-2781

904 Huang L, Xu A-M, Liu W (2015) Transglutaminase 2 in cancer. *Am J Cancer Res* 5: 2756-2776

905 Hwang JY, Mangala LS, Fok JY, Lin YG, Merritt WM, Spannuth WA, Nick AM, Fiterman DJ, Vivas-  
906 Mejia PE, Deavers MT, Coleman RL, Lopez-Berestein G, Mehta K, Sood AK (2008) Clinical and

- 907 Biological Significance of Tissue Transglutaminase in Ovarian Carcinoma. *Cancer Res* 68: 5849-  
908 5858
- 909 Ientile R, Curro M, Caccamo D (2015) Transglutaminase 2 and neuroinflammation. *Amino*  
910 *Acids* 47: 19-26
- 911 Iismaa SE, Mearns BM, Lorand L, Graham RM (2009) Transglutaminases and disease: lessons  
912 from genetically engineered mouse models and inherited disorders. *Physiol Rev* 89: 991-1023
- 913 Illingworth M, Ramsey A, Zheng Z, Chen L (2011) Stimulating the Substrate Folding Activity of  
914 a Single Ring GroEL Variant by Modulating the Cochaperonin GroES. *J Biol Chem* 286: 30401-  
915 30408
- 916 Jackson SP, Tjian R (1988) O-glycosylation of eukaryotic transcription factors: implications for  
917 mechanisms of transcriptional regulation. *Cell* 55: 125-133
- 918 Józwiak P, Forma E, Bryś M, Krzeslak A (2014) O-GlcNAcylation and Metabolic Reprogramming  
919 in Cancer. *Frontiers in endocrinology* 5: 145
- 920 Keresztessy Z, Csoz E, Harsfalvi J, Csomos K, Gray J, Lightowers RN, Lakey JH, Balajthy Z, Fesus  
921 L (2006) Phage display selection of efficient glutamine-donor substrate peptides for  
922 transglutaminase 2. *Protein Sci* 15: 2466-80
- 923 Kreppel LK, Hart GW (1999) Regulation of a Cytosolic and Nuclear O-GlcNAc Transferase: ROLE  
924 OF THE TETRATRICOPEPTIDE REPEATS. *J Biol Chem* 274: 32015-32022
- 925 Kumar S, Donti TR, Agnihotri N, Mehta K (2014) Transglutaminase 2 reprogramming of glucose  
926 metabolism in mammary epithelial cells via activation of inflammatory signaling pathways. *Int*  
927 *J Cancer* 134: 2798-807
- 928 Lee JH, Jeong J, Jeong EM, Cho SY, Kang JW, Lim J, Heo J, Kang H, Kim IG, Shin DM (2014)  
929 Endoplasmic reticulum stress activates transglutaminase 2 leading to protein aggregation. *Int*  
930 *J Mol Med* 33: 849-55
- 931 Lee JK, Enciso GA, Boassa D, Chander CN, Lou TH, Pairawan SS, Guo MC, Wan FYM, Ellisman  
932 MH, Sütterlin C, Tan M (2017) Replication-dependent size reduction precedes differentiation  
933 in *Chlamydia trachomatis*. *Nature Comm*: 1-9
- 934 Lee KN, Maxwell MD, Patterson MK, Birckbichler PJ, Conway E (1992) Identification of  
935 transglutaminase substrates in HT29 colon cancer cells: use of 5-(biotinamido)pentylamine as  
936 a transglutaminase-specific probe. *Biochimica et Biophysica Acta (BBA) - Molecular Cell*  
937 *Research* 1136: 12-16
- 938 Li Y, Roux C, Lazereg S, LeCaer JP, Laprevote O, Badet B, Badet-Denisot MA (2007)  
939 Identification of a novel serine phosphorylation site in human glutamine:fructose-6-  
940 phosphate amidotransferase isoform 1. *Biochemistry (Mosc)* 46: 13163-9
- 941 Liechti G, Kuru E, Packiam M, Hsu Y-P, Tekkam S, Hall E, Rittichier JT, VanNieuwenhze M, Brun  
942 YV, Maurelli AT (2016) Pathogenic *Chlamydia* Lack a Classical Sacculus but Synthesize a



943 Narrow, Mid-cell Peptidoglycan Ring, Regulated by MreB, for Cell Division. *PLoS Pathog* 12:  
944 e1005590

945 Liu C, Kellems RE, Xia Y (2017) Inflammation, Autoimmunity, and Hypertension: The Essential  
946 Role of Tissue Transglutaminase. *Am J Hypertens* 30: 756-764

947 Majeed M, Krause KH, Clark RA, Kihlström E, Stendahl O (1999) Localization of intracellular  
948 Ca<sup>2+</sup> stores in HeLa cells during infection with *Chlamydia trachomatis*. *J Cell Sci* 112: 35-44

949 Mehul B, Bawumia S, Hughes RC (1995) Cross-linking of galectin 3, a galactose-binding protein  
950 of mammalian cells, by tissue-type transglutaminase. *FEBS Lett* 360: 160-4

951 Nelea V, Nakano Y, Kaartinen MT (2008) Size distribution and molecular associations of plasma  
952 fibronectin and fibronectin crosslinked by transglutaminase 2. *The protein journal* 27: 223-33

953 Nurminskaya M, Beazley KE, Smith EP, Belkin AM (2014) Transglutaminase 2 promotes PDGF-  
954 mediated activation of PDGFR/Akt1 and beta-catenin signaling in vascular smooth muscle cells  
955 and supports neointima formation. *J Vasc Res* 51: 418-28

956 Ojcius D, Degani H, Mispelter J, Dautry-Varsat A (1998) Enhancement of ATP levels and glucose  
957 metabolism during an infection by *Chlamydia*. *J Biol Chem* 273: 7052-8

958 Olson MG, Widner RE, Jorgenson LM, Lawrence A, Lagundzin D, Woods NT, Ouellette SP, Rucks  
959 EA (2019) Proximity Labeling To Map Host-Pathogen Interactions at the Membrane of a  
960 Bacterium-Containing Vacuole in *Chlamydia trachomatis*-Infected Human Cells. *Infect Immun*  
961 87

962 Orrù S, Caputo I, D'Amato A, Ruoppolo M, Esposito C (2003) Proteomics Identification of Acyl-  
963 acceptor and Acyl-donor Substrates for Transglutaminase in a Human Intestinal Epithelial Cell  
964 Line: IMPLICATIONS FOR CELIAC DISEASE. *J Biol Chem* 278: 31766-31773

965 Palucci I, Matic I, Falasca L, Minerva M, Maulucci G, De Spirito M, Petruccioli E, Goletti D,  
966 Rossin F, Piacentini M, Delogu G (2017) Transglutaminase type 2 plays a key role in the  
967 pathogenesis of *Mycobacterium tuberculosis* infection. *J Intern Med*

968 Peng B, Lu C, Tang L, Yeh IT, He Z, Wu Y, Zhong G (2011) Enhanced upper genital tract  
969 pathologies by blocking Tim-3 and PD-L1 signaling pathways in mice intravaginally infected  
970 with *Chlamydia muridarum*. *BMC infectious diseases* 11: 347

971 Pincus JH, Waelsch H (1968) The specificity of transglutaminase. I. Human hemoglobin as a  
972 substrate for the enzyme. *Arch Biochem Biophys* 126: 34-43

973 Pounds S, Cheng C (2006) Robust estimation of the false discovery rate. *Bioinformatics* 22:  
974 1979-87

975 Rasmussen SJ, Eckmann L, Quayle AJ, Shen L, Zhang Y-X, Anderson DJ, Fierer J, Stephens R,  
976 Kagnoff M (1997) Secretion of proinflammatory cytokines by epithelial cells in response to  
977 *Chlamydia* infection suggests a central role for epithelial cells in chlamydial pathogenesis. *J*  
978 *Clin Invest* 99: 77-87

- 979 Read T, Brunham R, Shen C, Gill S, Heidelberg J, White O, Hickey E, Peterson J, Utterback T,  
980 Berry K, Bass S, Linher K, Weidman J, Khouri H, Craven B, Bowman C, Dodson R, Gwinn M,  
981 Nelson W, DeBoy R et al. (2000) Genome sequences of *Chlamydia trachomatis* MoPn and  
982 *Chlamydia pneumoniae* AR39. *Nucleic Acids Res* 28: 1397-1406
- 983 Ritchie ME, Phipson B, Wu D, Hu Y, Law CW, Shi W, Smyth GK (2015) limma powers differential  
984 expression analyses for RNA-sequencing and microarray studies. *Nucleic Acids Res* 43: e47
- 985 Rossin F, D'Eletto M, Macdonald D, Farrace MG, Piacentini M (2012) TG2 transamidating  
986 activity acts as a reostat controlling the interplay between apoptosis and autophagy. *Amino*  
987 *Acids* 42: 1793-802
- 988 Roth A, Konig P, van Zandbergen G, Klinger M, Hellwig-Burgel T, Daubener W, Bohlmann MK,  
989 Rupp J (2010) Hypoxia abrogates antichlamydial properties of IFN-gamma in human fallopian  
990 tube cells in vitro and ex vivo. *Proc Natl Acad Sci U S A* 107: 19502-7
- 991 Rother M, Gonzalez E, Teixeira da Costa AR, Wask L, Gravenstein I, Pardo M, Pietzke M,  
992 Gurumurthy RK, Angermann J, Laudeley R, Glage S, Meyer M, Chumduri C, Kempa S, Dinkel K,  
993 Unger A, Klebl B, Klos A, Meyer TF (2018) Combined Human Genome-wide RNAi and  
994 Metabolite Analyses Identify IMPDH as a Host-Directed Target against *Chlamydia* Infection.  
995 *Cell Host Microbe* 23: 661-671.e8
- 996 Russell DG, VanderVen BC, Lee W, Abramovitch RB, Kim M-j, Homolka S, Niemann S, Rohde  
997 KH (2010) Mycobacterium tuberculosis Wears What It Eats. *Cell Host & Microbe* 8: 68-76
- 998 Schmittgen TD, Livak KJ (2008) Analyzing real-time PCR data by the comparative CT method.  
999 *Nature Protocols* 3: 1101-1108
- 1000 Scidmore MA (2005) Cultivation and laboratory maintenance of *Chlamydia trachomatis*. *Curr*  
1001 *Protocols Microbiol*: 11A1.1-11A1.25
- 1002 Shao M, Cao L, Shen C, Satpathy M, Chelladurai B, Bigsby RM, Nakshatri H, Matei D (2009)  
1003 Epithelial-to-Mesenchymal Transition and Ovarian Tumor Progression Induced by Tissue  
1004 Transglutaminase. *Cancer Res* 69: 9192-9201
- 1005 Sharma M, Machuy N, Bohme L, Karunakaran K, Maurer AP, Meyer TF, Rudel T (2011) HIF-  
1006 1alpha is involved in mediating apoptosis resistance to *Chlamydia trachomatis*-infected cells.  
1007 *Cell Microbiol* 13: 1573-85
- 1008 Shi L, Salamon H, Eugenin EA, Pine R, Cooper A, Gennaro ML (2015) Infection with  
1009 Mycobacterium tuberculosis induces the Warburg effect in mouse lungs. *Scientific reports* 5:  
1010 18176
- 1011 Sohn J, Chae JB, Lee SY, Kim SY, Kim JG (2010) A novel therapeutic target in inflammatory  
1012 uveitis: transglutaminase 2 inhibitor. *Korean J Ophthalmol* 24: 29-34
- 1013 Stephens RS, Kalman S, Lammel C, Fan J, Marathe R, Aravind L, Mitchell W, Olinger L, Tatusov  
1014 RL, Zhao Q, Koonin EV, Davis RW (1998) Genome sequence of an obligate intracellular  
1015 pathogen of humans: *Chlamydia trachomatis*. *Science* 282: 754-755

1016 Sugimura Y, Hosono M, Wada F, Yoshimura T, Maki M, Hitomi K (2006) Screening for the  
1017 preferred substrate sequence of transglutaminase using a phage-displayed peptide library:  
1018 identification of peptide substrates for TGASE 2 and Factor XIIIa. *J Biol Chem* 281: 17699-706

1019 Suto N, Ikura K, Sasaki R (1993) Expression induced by interleukin-6 of tissue-type  
1020 transglutaminase in human hepatoblastoma HepG2 cells. *J Biol Chem* 268: 7469-73

1021 Tarbet HJ, Dolat L, Smith TJ, Condon BM, O'Brien ET, 3rd, Valdivia RH, Boyce M (2018) Site-  
1022 specific glycosylation regulates the form and function of the intermediate filament  
1023 cytoskeleton. *Elife* 7

1024 Tyanova S, Temu T, Cox J (2016) The MaxQuant computational platform for mass  
1025 spectrometry-based shotgun proteomics. *Nat Protoc* 11: 2301-2319

1026 Vromman F, Laverriere M, Perrinet S, Dufour A, Subtil A (2014) Quantitative Monitoring of the  
1027 *Chlamydia trachomatis* Developmental Cycle Using GFP-Expressing Bacteria, Microscopy and  
1028 Flow Cytometry. *PLoS One* 9: e99197

1029 Wang X, Hybiske K, Stephens RS (2017) Orchestration of the mammalian host cell glucose  
1030 transporter proteins-1 and 3 by *Chlamydia* contributes to intracellular growth and infectivity.  
1031 *Pathog Dis* 75

1032 Wieczorek S, Combes F, Lazar C, Giai Gianetto Q, Gatto L, Dorffer A, Hesse AM, Coute Y, Ferro  
1033 M, Bruley C, Burger T (2017) DAPAR & ProStaR: software to perform statistical analyses in  
1034 quantitative discovery proteomics. *Bioinformatics* 33: 135-136

1035 Yang X, Qian K (2017) Protein O-GlcNAcylation: emerging mechanisms and functions. *Nat Rev*  
1036 *Mol Cell Biol* 18: 452-465

1037 Zibrova D, Vandermoere F, Göransson O, Peggie M, Mariño KV, Knierim A, Spengler K, Weigert  
1038 C, Viollet B, Morrice NA, Sakamoto K, Heller R (2017) GFAT1 phosphorylation by AMPK  
1039 promotes VEGF-induced angiogenesis. *Biochem J* 474: 983-1001  
1040  
1041

1042 LEGENDS TO THE FIGURES

1043

1044 Figure 1. **TG2 transamidase activity increases during *C. trachomatis* infection along with its**  
1045 **expression.**

1046 A – Whole cell lysates were prepared with HeLa cells infected or not for 48 h with *C.*  
1047 *trachomatis* L2 (multiplicity of infection MOI=1) in the presence or not of BP. In the indicated  
1048 samples CP4d was added 2 h before infection. Cell lysates were run on SDS-PAGE, proteins  
1049 were transferred to a membrane and BP incorporation was revealed with HRP-conjugated  
1050 streptavidin. BP incorporation is enhanced in infected samples, and is inhibited by CP4d. The  
1051 two main bands present in all samples correspond to naturally biotinylated host proteins  
1052 (Haneji & Koide, 1989). After blotting the membrane was stained with Coomassie blue to  
1053 control for equal loading.

1054 B – Same as in (A), except that where indicated 250  $\mu$ M doxycycline (doxy, left) or 7  $\mu$ M  
1055 cycloheximide (CHX, right) were added 24 h or 2 hpi, respectively.

1056 C – Whole cell lysates were prepared with TG2<sup>+/+</sup> and TG2<sup>-/-</sup> MEFs infected or not for 48 h with  
1057 *C. trachomatis* L2 in the presence or not of BP, and analyzed as in (A).

1058 D –Western blot with anti-TG2 antibodies on total cell lysates infected or not with *C.*  
1059 *trachomatis* L2 for the indicated time. The histogram displays the **quantification** [HG1] **mean  $\pm$**   
1060 **SD** of TG2 expression relative to actin from four independent experiments, with the results of  
1061 the Student's ratio-paired t-test. NI: not infected.

1062 E – Cells were infected with *C. trachomatis* L2 (MOI=1) for 24 or **4846** [HG2] h. Where indicated,  
1063 40  $\mu$ M CP4d was added 2 hpi. *tgm2* transcripts were measured by real-time RT-PCR and  
1064 normalized to *actin* transcripts following the  $\Delta\Delta$ Ct method. The data are presented as relative  
1065 mRNA levels compared to uninfected cells and shown as the mean  $\pm$  SD. Each experiment was  
1066 performed in duplicate and repeated at least four times. P-values of Student's ratio-paired t-  
1067 test <0.05 are shown.

1068 F – Cells were treated for 18 h with the indicated concentration of human recombinant IL-6  
1069 before measuring TG2 transcription relative to actin like in (E). **The data are presented as**  
1070 **relative mRNA levels compared to untreated cells and shown as the mean  $\pm$  SD. Each**  
1071 **experiment was performed in duplicate and repeated at least **fourthree** times. P-values of**  
1072 **Student's ratio-paired t-test <0.05 are shown.** [HG3]

1073 F – Cells were left uninfected or infected with *C. trachomatis* L2 in the presence of the  
1074 indicated concentration of anti-IL-6 receptor antibodies. Forty-eight h later TG2 transcription  
1075 relative to actin was measured like in (E). **The data are presented as relative mRNA levels**  
1076 **compared to uninfected/untreated cells and shown as the mean  $\pm$  SD. Each experiment was**  
1077 **performed in duplicate and repeated at least **fourthree** times. P-values of Student's ratio-**  
1078 **paired t-test <0.05 are shown.** [HG4]

1079

1080 Figure 2. **TG2 activity is needed for optimal *C. trachomatis* developmental and enhances**  
1081 **hydrosalpinx upon *C. muridarum* infection in mice.**

1082 A – HeLa cells were pre-treated with the indicated concentrations of CP4d (or DMSO alone)  
1083 for 2 h before being infected with L2<sup>incD</sup>GFP at MOI=0.15. Thirty hours later the cells were  
1084 disrupted and bacterial titers (IFU=inclusion forming unit) were determined by re-infecting  
1085 fresh HeLa cells as described in the methods. The mean  $\pm$  SD of three independent  
1086 experiments are shown. P-values of Student's paired t-test are indicated when <0.05.

1087 B – HeLa cells were transfected with control siRNA or two siRNAs against TG2. Two days later,  
1088 the efficiency of the silencing was assessed by western blot using anti-TG2 antibodies and anti-

1089 actin antibodies as loading control (bottom). Duplicate wells were infected with L2<sup>incD</sup>GFP and  
1090 progeny was analyzed as in (A) (top). The mean ± SD of four independent experiments are  
1091 shown. P-values of Student's paired t-test are indicated when <0.05.<sup>[HG5]</sup>

1092 C – Same as in (A) except that *C. trachomatis* serovar L2 (left) or D (right) were grown in  
1093 primary cells isolated from fallopian tubes. For serovar D, IFU were determined 48 hpi. The  
1094 mean ± SD of four to five independent experiments are shown. P-values of Student's paired t-  
1095 test are indicated when <0.05.<sup>[HG6]</sup>

1096 D – HeLa cells were pre-treated with the indicated concentrations of CP4d (or DMSO alone)  
1097 for 2 h before being infected with L2<sup>incD</sup>GFP at MOI=0.15. Thirty hours later the cells were fixed  
1098 and analyzed by flow cytometry. The percentage of infected cells (left) and the mean  
1099 fluorescence of the infected population (right) ± SD <sup>[HG7]</sup> are shown for three independent  
1100 experiments. P-values of Student's paired t-test are indicated when <0.05.<sup>[HG8] [HG9]</sup> A  
1101 representative field for each condition is shown, scale bar = 10 μm<sup>[HG10]</sup>.

1102 E<sup>[HG11]</sup> – Primary epithelial cells isolated from fallopian tubes were pre-treated with the  
1103 indicated concentrations of CP4d (or DMSO alone) for 2 h before being infected with *C.*  
1104 *trachomatis* serovar L2 (left) or D (right). Twenty-four hours later the cells were fixed, bacteria  
1105 were stained using FITC-labeled anti-Chlamydia-LPS antibodies, and the mean size of the  
1106 inclusions manually determined using ImageJ, on twenty inclusions per experiment. The mean  
1107 ± SD of three independent experiments are shown. P-values of Student's paired t-test are  
1108 indicated when <0.05.<sup>[HG12] [HG13]</sup>

1109 F<sup>[HG14]</sup> – Mice were infected intravaginally with 10<sup>5</sup> IFU of *C. muridarum*. Twenty-five days later  
1110 the mice were sacrificed and the upper genital tract, from the uterine horn to the oviduct, was  
1111 collected. The right part was used for bacterial burden assessment (top left). The left part was  
1112 rinsed with PBS and observed with a binocular magnifier (right) to determine the hydrosalpinx  
1113 score (bottom left). Each dot represents one mouse, the mean ± SD is shown. P-values of  
1114 Mann-Whitney test are indicated when <0.05.

1115  
1116 **Figure 3. TG2 controls glucose import.**

1117 A – MEFs were grown for 24 h culture medium complemented with the indicated  
1118 concentration of glucose before being infected with L2<sup>incD</sup>GFP bacteria (MOI = 0.2). Cells were  
1119 disrupted 30 h later and the bacterial titer determined by re-infecting fresh wild type cells.  
1120 The mean ± SD of three independent experiments are shown.

1121 B – Cells were infected with *C. trachomatis* L2 (MOI=1) for 24 or 48 h. Where indicated 40 μM  
1122 CP4d was added 2 hpi. *GLUT-1* and *GLUT-3* transcripts were measured by real-time RT-PCR  
1123 and normalized to *actin* transcripts following the ΔΔCt method. The data are presented as  
1124 relative mRNA levels compared to uninfected cells and shown as the mean ± SD. Each  
1125 experiment was performed in duplicate and repeated four times. P-values of Student's ratio-  
1126 paired t-test are indicated when <0.05.

1127 C – Relationship between *TGM2* and *GLUT-1* (top) and *GLUT-3* (bottom) expression across  
1128 265 HGSOcs. Expression comparisons were performed using Spearman's rank correlation test.

1129 D<sup>[HG15]</sup> – HeLa cells were infected with *C. trachomatis* L2 (MOI=1) for 24 or 46 h. *HIF-1α*  
1130 transcripts were measured by real-time RT-PCR and normalized to *actin* transcripts. The data  
1131 are presented as relative mRNA levels compared to uninfected cells and shown as the mean  
1132 ± SD. Each experiment was performed in duplicate and repeated three times. P-values of  
1133 Student's ratio-paired t-test are > 0.05.

1134

1135 E<sub>[HG16]</sub> — HeLa cells were transfected with control siRNA or two siRNAs against HIF-1 $\alpha$ . Two  
1136 days later, cells were infected with *C. trachomatis* L2 (MOI=1) for 48 h. The indicated  
1137 transcripts were measured by real-time RT-PCR and normalized to *actin* transcripts. The data  
1138 are presented as relative mRNA levels compared to uninfected cells and shown as the mean  
1139  $\pm$  SD. Each experiment was performed in duplicate and repeated three times. P-values of  
1140 Student's ratio-paired t-test are indicated when <0.05.

1141  
1142 F<sub>[HG17]</sub> — TG2<sup>-/-</sup> MEFs stably transformed or not with the indicated TG2 construct were infected  
1143 for two days with *C. trachomatis* L2 (MOI=1). Mouse *GLUT-1* transcripts were measured by  
1144 real-time RT-PCR and normalized to mouse *actin* transcripts. The data are presented as  
1145 relative mRNA levels compared to uninfected cells and shown as the mean  $\pm$  SD. Each  
1146 experiment was performed in duplicate and repeated three times. P-values of Student's ratio-  
1147 paired t-test are indicated when <0.05.

1148  
1149  
1150 **Figure 4. GFPT is a substrate of TG2 transamidase activity.**

1151 A – HeLa cells were infected with *C. trachomatis* (MOI = 1) and 40  $\mu$ M CP4d was added or not  
1152 2 hpi. After 24 h 0.5 mM BP was added and cells were lysed at 48 hpi. Lysates were  
1153 precipitated with streptavidin-coated beads. After separation with SDS-PAGE, proteins were  
1154 transferred to a membrane and blotted with anti-GFPT antibody followed with HRP-  
1155 conjugated secondary antibody.

1156 B – *In vitro* assay testing the ability of purified TG2 to crosslink purified rhGFPT1 with BP.  
1157 Samples were incubated for 3 h at 37°C before separation by SDS-PAGE. Proteins were  
1158 transferred to a membrane and BP was revealed using HRP-conjugated streptavidin. rhGFPT1  
1159 is 77.5 kDa.

1160 C –GFPT1 sequence: glutamine residues identified by mass spectrometry as cross-linked to BP  
1161 are in bold letter .

1162 D – *In vitro* assay was performed as described in B using wild type rhGFPT1 (WT), rhGFPT1  
1163 Q58N, rhGFPT1 Q328N or rhGFPT1 Q555N as substrates. The reaction was performed at 37 °C  
1164 for 30 min. After probing with HRP-Streptavidin the membrane was washed and probed with  
1165 anti-GFPT antibodies followed with HRP-conjugated secondary antibodies. The ratio of  
1166 modified protein (streptavidin signal) to the total GFPT is shown, normalized to its value with  
1167 WT rhGFPT1. The mean  $\pm$  SD <sub>[HG18]</sub> of five independent experiments is shown, the p-value of  
1168 the Student's ratio-paired t-test is indicated when <0.05.

1169 E – Lysates of cells treated or not for 6 h with ionomycin were incubated at 37 °C for 45 min  
1170 with fructose-6-P and glutamine. The production of glucosamine-6-P was measured using  
1171 HPAEC-PAD. Results of three independent experiments are shown, with mean,  $\pm$  SD, and p-  
1172 value of the Student's paired t-test is indicated (\*P < 0.05).

1173  
1174  
1175 **Figure 5. TG2 activation results in increased UDP-GlcNAc production.**

1176 A – Schematic view of the hexosamine biosynthesis pathway. Production of glucosamine-6-P  
1177 by GFPT is the first and rate-limiting step of the pathway that produces UDP-GlcNAc. HK:  
1178 hexokinase; G6PI: glucose-6-P isomerase; GFPT: glutamine:fructose-6-P amidotransferase;  
1179 GNA: glucosamine-6-P N-acetyltransferase; PGM3: phosphoglucomutase 3; UAP: UDP-N-  
1180 acetylglucosamine pyrophosphorylase; OGT: O-GlcNAc transferase OGA: O-GlcNAcase;  
1181 GlcNAc: N-acetylglucosamine.

1182 B – Endocervical epithelial cells were pre-treated or not with 40  $\mu$ M CP4d for 2 h before  
1183 addition of the indicated concentration of ionomycin (or an equivalent volume of DMSO) and  
1184 0.5  $\mu$ M BP. Six hours later whole cell lysates were analyzed by western blot. The membrane  
1185 was first blotted with HRP-conjugated streptavidin to detect TG2 activity, then extensively  
1186 washed and probed with anti-O-GlcNAcylation antibody followed with HRP-conjugated  
1187 secondary antibodies. Last the membrane was probed with anti-actin as a loading control.  
1188 C – The same experimental procedure as described in [B-\(B\)](#) was applied to HeLa cells treated  
1189 for 48 h prior to ionomycin treatment (8  $\mu$ M) with siRNA control or directed against TG2.

1190

1191 **Figure 6. Optimal bacterial growth requires GFPT and prevents UDP-GlcNAc accumulation.**

1192 A – HeLa cells were infected or not (NI) with *C. trachomatis* (MOI = 1), then lysed 24 or 48 hpi.  
1193 After separation with SDS-PAGE, proteins were transferred to a membrane, probed with anti-  
1194 O-GlcNAcylation antibody followed with HRP-conjugated secondary antibodies. After  
1195 extensive washes the membrane was blotted again with anti-GFPT and anti-actin antibodies  
1196 before revelation with HRP-conjugated secondary antibodies.

1197 B – HeLa cells were infected or not with *C. trachomatis* (MOI = 1). Twenty-four [hours](#) later, 8  
1198  $\mu$ M ionomycin (or DMSO alone) and 0.5 mM BP were added. After 6 h of treatment, cells were  
1199 lysed and proteins revealed as in [\(A\)](#).

1200 C – HeLa cells treated for 72 h with siRNA targeting GFPT1 or GFPT2 were lysed. After  
1201 separation with SDS-PAGE, proteins were transferred to a membrane, probed with anti-GFPT  
1202 and anti-actin antibody before revelation with HRP-conjugated secondary antibodies.

1203 D – HeLa cells were transfected with control siRNA or siRNAs against GFPT or TG2. Two days  
1204 later the cells were infected for the indicated times (MOI=0.3) before fixation, rupture of the  
1205 cells and measurement of bacterial diameter. The mean diameter  $\pm$  SD and p-values of  
1206 Student's paired t-test on 4 independent experiments are shown.

1207 E – HeLa cells treated for 48 h with siRNA targeting GFPT1 or not (siCTRL) were infected with  
1208 *C. trachomatis* (MOI = 0.15). Thirty hours later cells were fixed and analyzed by flow  
1209 cytometry. The percentage of infected cells (top) and the mean fluorescence of the infected  
1210 population (middle) )  $\pm$  SD [\[HG19\]](#) are shown for at least four independent experiments.  
1211 Duplicate wells were lysed and used to re-infect fresh HeLa cells to determine the bacterial  
1212 titer (bottom). P-values of Student's ratio-paired t-test are indicated.

1213 F – Schematic view of the outcome of TG2 activation in infection. The increase in TG2  
1214 expression and activity in cells infected with *C. trachomatis* results in the up-regulation of the  
1215 expression of glucose transporters. Increasing quantities of glucose are thus imported in the  
1216 host cytoplasm and redirected to the vacuole, where they fuel bacterial growth. Parallel to  
1217 this transcriptional outcome, the transamidating activity of TG2 targets the host enzyme GFPT,  
1218 thereby boosting the hexosamine biosynthesis pathway. The bacteria consume the resulting  
1219 UDP-GlcNAc, or an intermediate along this pathway, in particular to sustain bacterial division.

1220

1221 Expanded View Figure Legends

1222

1223

1224 **Figure EV1. TG2 is beneficial for bacterial development.**— [Related](#) ([related](#) to Figure 2).

1225 A – HeLa cells were pre-treated with the indicated concentrations of Cysteamine for 2 h before  
1226 being infected with L2<sup>incD</sup>GFP at MOI=0.15. Thirty hours later the cells were disrupted and  
1227 bacterial titers (IFU) were determined by re-infecting fresh HeLa cells as described in the

1228 methods. The mean  $\pm$  SD of three independent experiments are shown. P-values of Student's  
1229 paired t-test are indicated when  $<0.05$ .

1230 B – TG2<sup>+/+</sup> and TG2<sup>-/-</sup> MEFs were infected with L2<sup>incD</sup>GFP at MOI=0.15. Thirty h later the cells  
1231 were disrupted and bacterial titers were determined by re-infecting fresh TG2<sup>+/+</sup> cells as  
1232 described in the methods. The mean  $\pm$  SD of five independent experiments and p-values from  
1233 Student's paired t-test [HG20] are shown.

1234 C – To measure bacterial adhesion TG2<sup>+/+</sup> and TG2<sup>-/-</sup> MEFs were incubated at 4 °C for 4 h with  
1235 L2<sup>incD</sup>GFP at MOI=10 before being washed and fixed as described in the methods. The mean  $\pm$   
1236 SD of three independent experiments are shown.

1237 D – TG2<sup>+/+</sup> and TG2<sup>-/-</sup> MEFs were infected with L2<sup>incD</sup>GFP at MOI=10 and fixed at the indicated  
1238 time. Extracellular bacteria were differentially labeled as described in the methods. The mean  
1239  $\pm$  SD of three independent experiments, and p-values from Student's paired t-test, are shown.

1240  
1241 **Figure EV2. Infection by *C. muridarum* activates TG2, which favors bacterial growth.—**  
1242 **Related (related to Figure 2).**

1243 A – Whole cell lysates were prepared with HeLa cells infected or not for 48 h with *C.*  
1244 *muridarum* (MOI=1) in the presence or not of BP. Cell lysates were run on SDS-PAGE, proteins  
1245 were transferred to a membrane and BP incorporation was revealed with HRP-conjugated  
1246 streptavidin.

1247 B – HeLa cells were transfected with siRNA against TG2 for 48 h before being infected in  
1248 duplicates with *C. muridarum* at MOI=0.15. Thirty hours later one set of cells were disrupted  
1249 and bacterial titers (IFU=inclusion forming unit) were determined by re-infecting fresh HeLa  
1250 cells as described in the methods. The mean  $\pm$  SD of three independent experiments and p-  
1251 values of Student's paired t-test are shown (top). Duplicate wells were incubated further for  
1252 a total of 48 h before the cells were fixed, permeabilized with 0.3% Triton-X100 and stained  
1253 with rabbit antibodies against *C. muridarum* GroEL followed with A488-coupled anti-rabbit  
1254 secondary antibodies. Samples were analyzed by flow cytometry, the percentage of infected  
1255 cells (middle) and the mean fluorescence of the infected population (bottom)  $\pm$  SD [HG21] are  
1256 shown for three independent experiments, p-values of Student's paired t-test are indicated.

1257  
1258 **Figure EV3. GFPT silencing affects bacterial division. Related (related to Figure 6).**

1259 HeLa cells treated for 48 h with siRNA targeting GFPT1 or not (siCTRL) were infected with *C.*  
1260 *trachomatis* (MOI = 1), fixed 30 hpi and processed for transmission electron microscopy. Lines  
1261 show example of measured RB diameters. Scale bar = 600 nm. RB diameters were measured  
1262 using ImageJ on > 300 bacteria in one experiment. Each dot represents one RB, t  
1263 he mean  
1264 value [HG22]  $\pm$  SD and p-value of Student's paired t-test are indicated.

1264  
1265



Figure 1

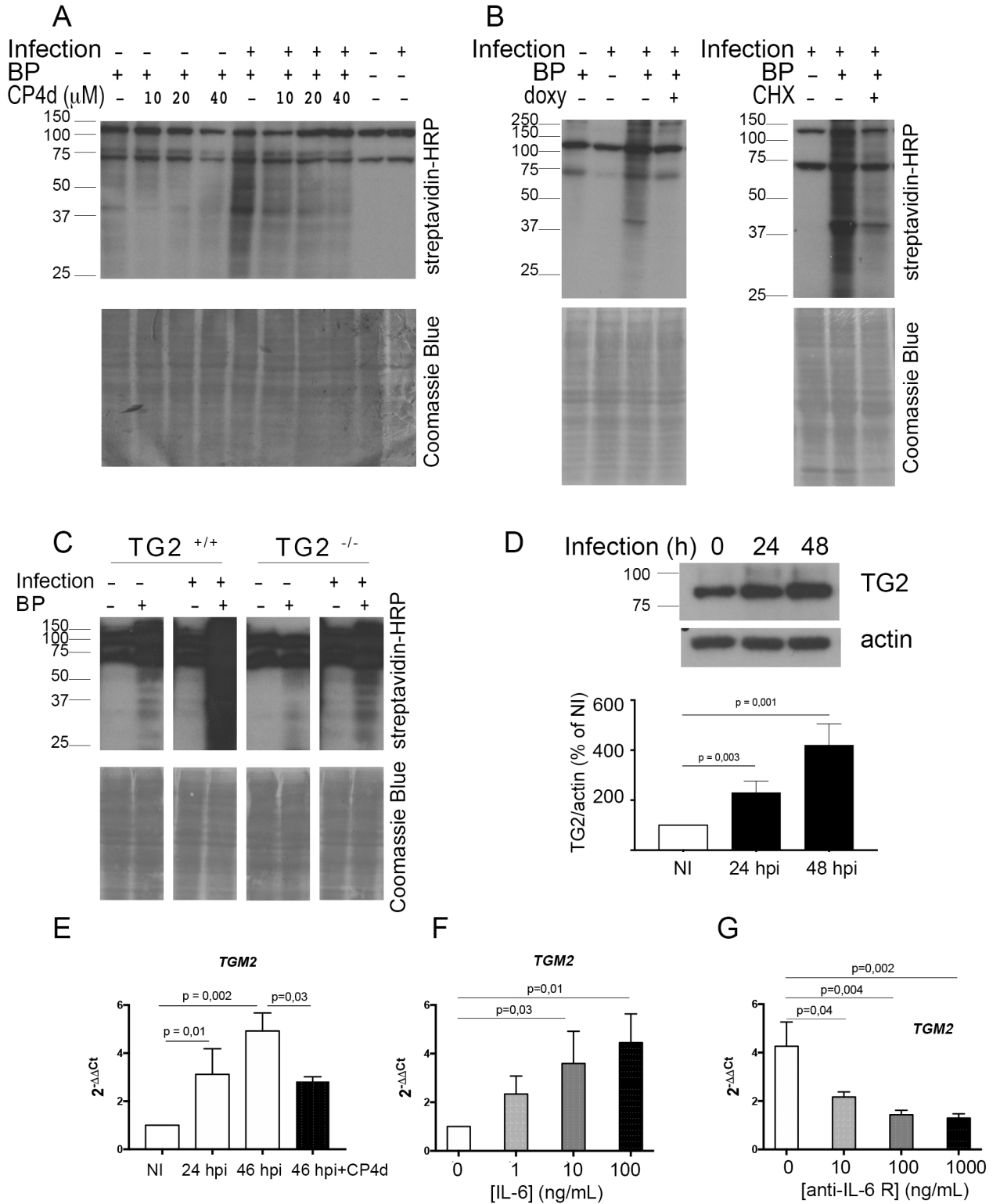


Figure 2

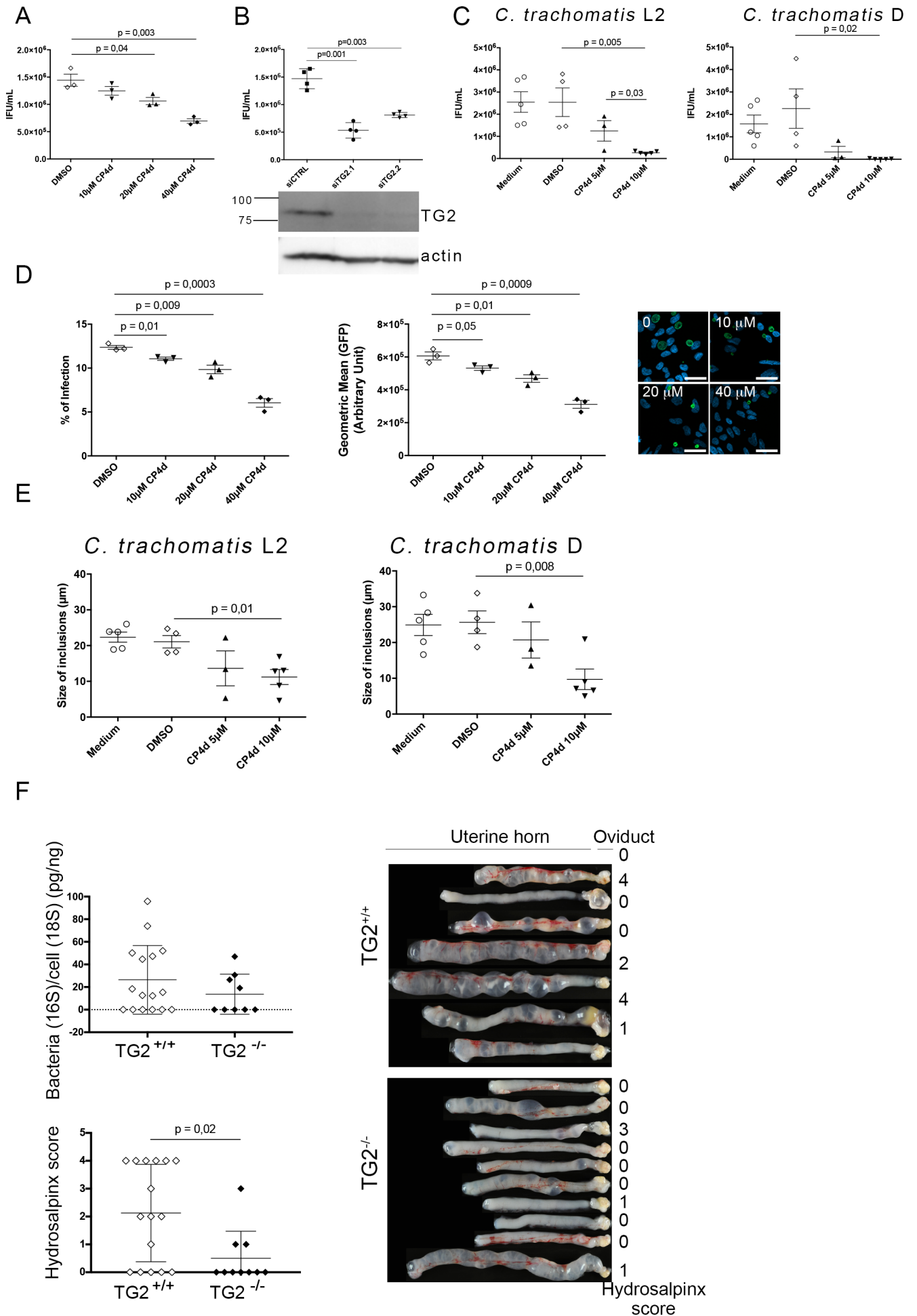
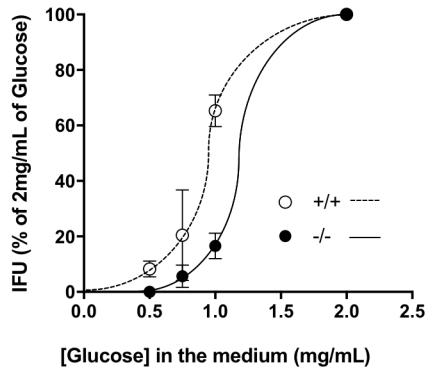


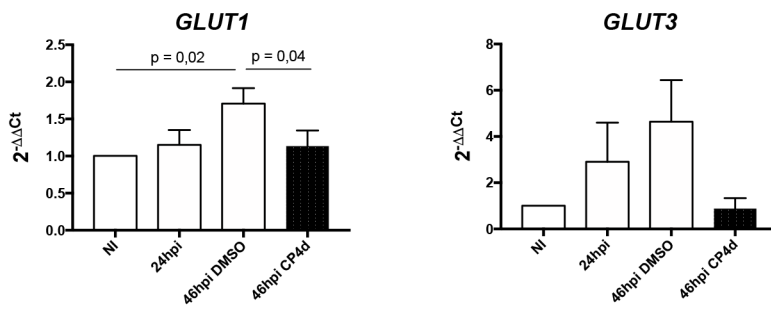
Figure 3

A

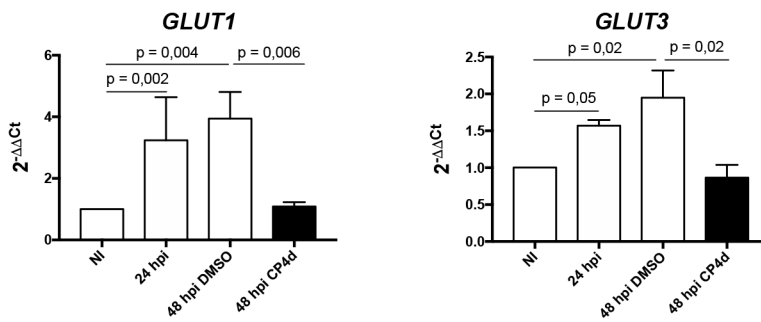


B

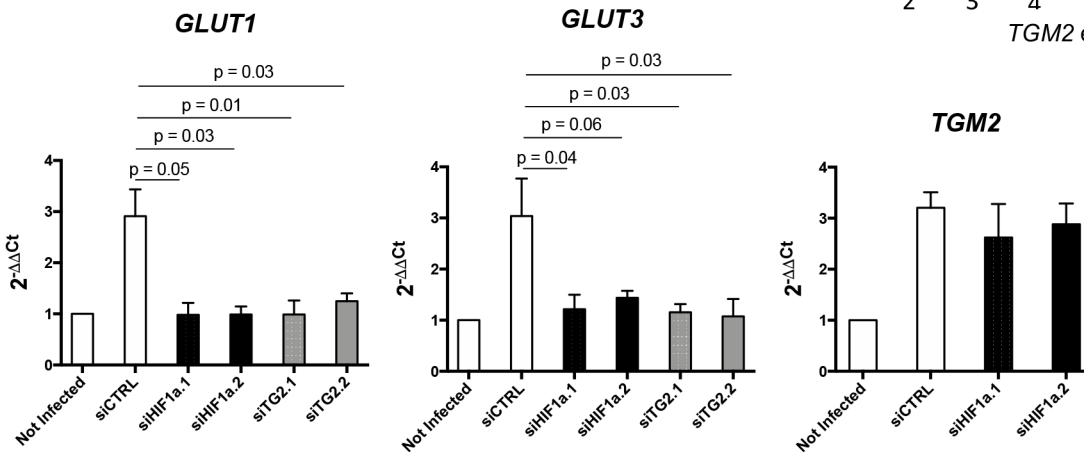
HeLa cells



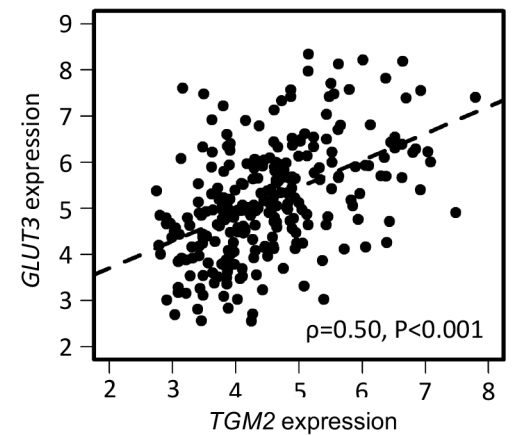
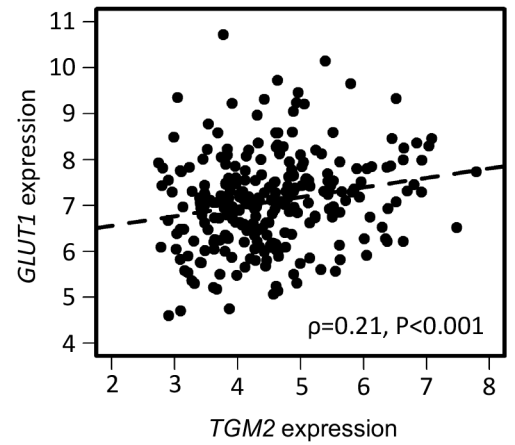
Primary epithelial cells



C



D



TGM2

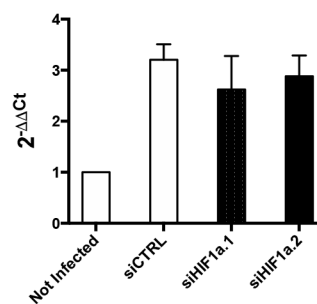


Figure 4

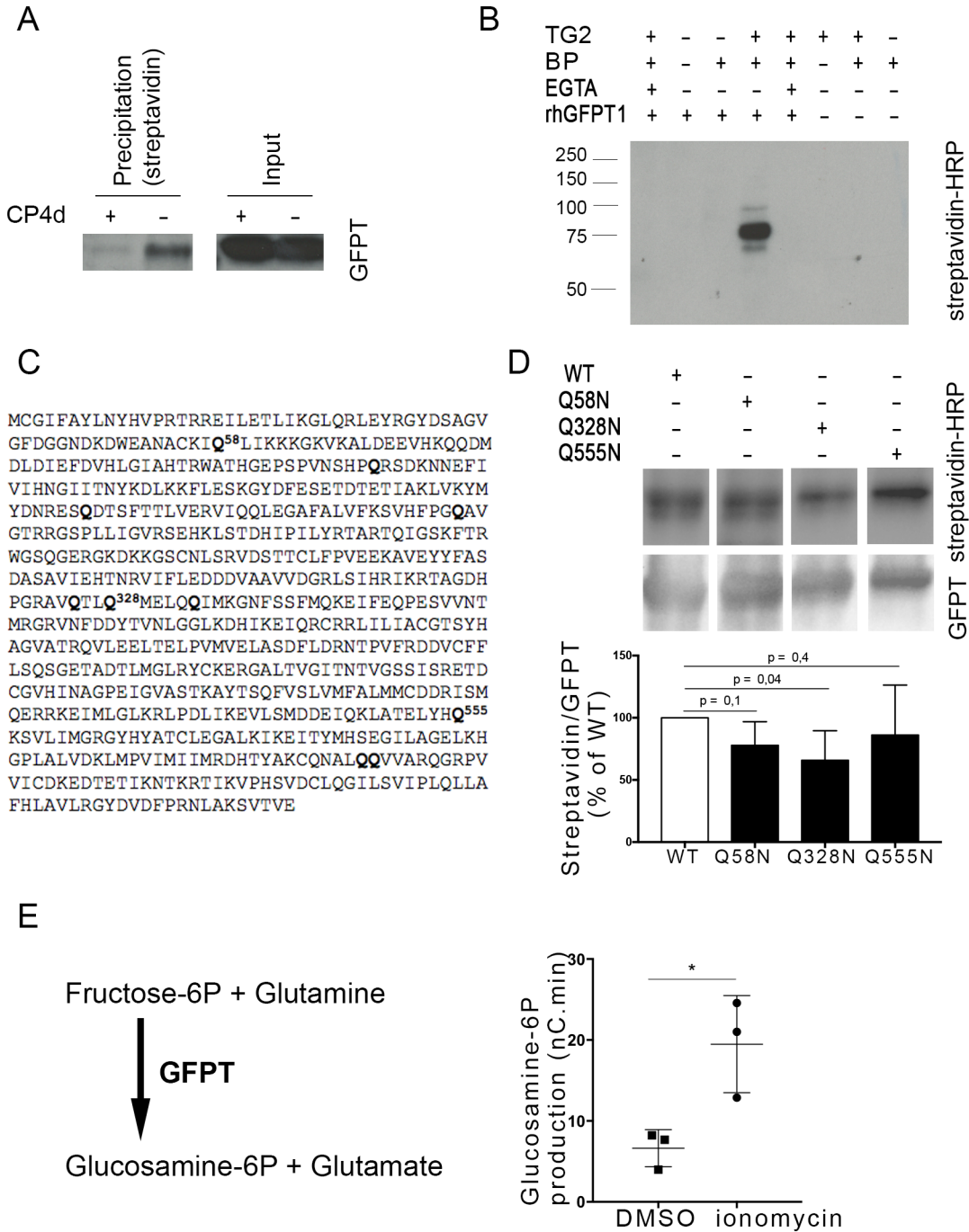


Figure 5

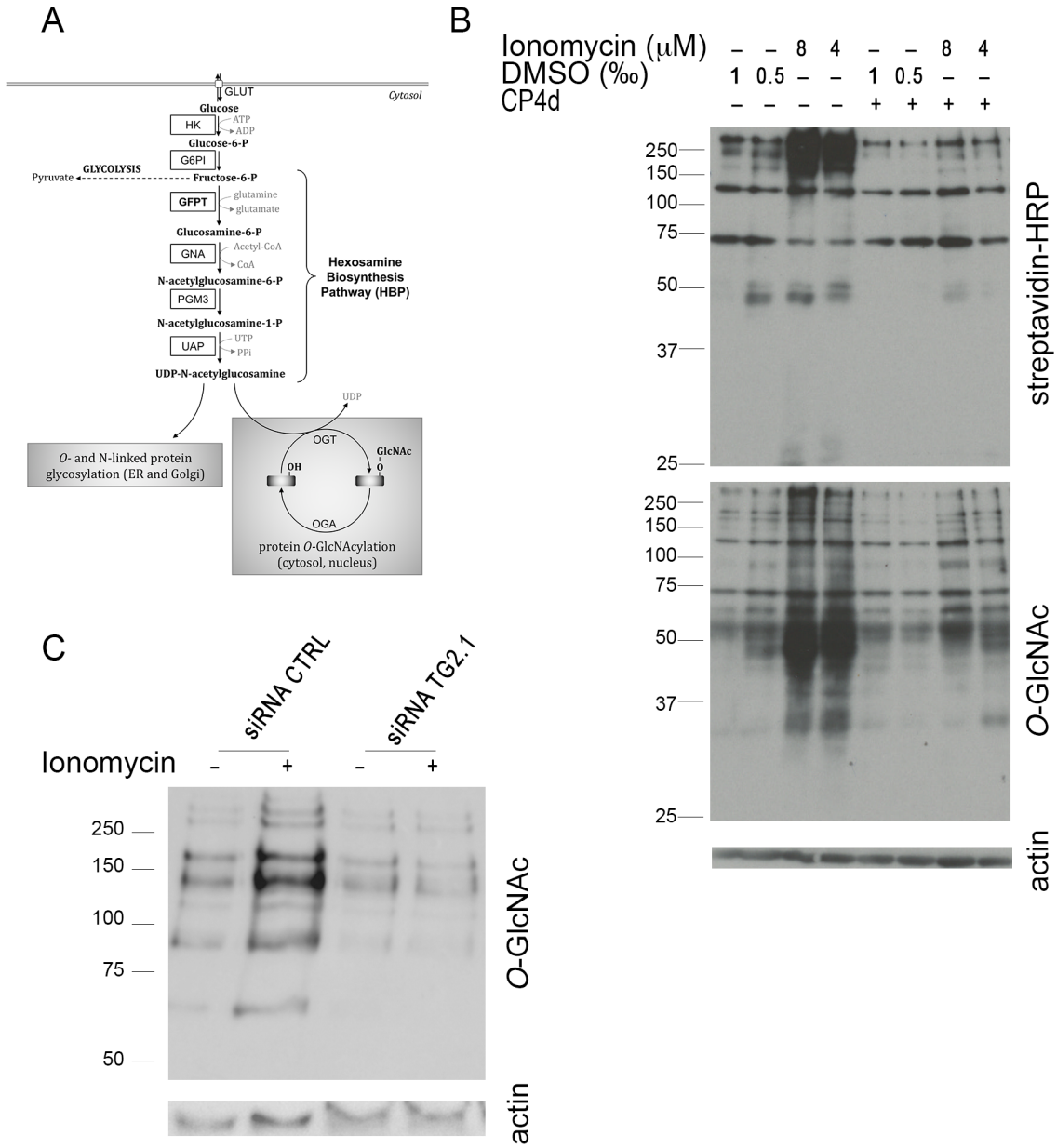


Figure 6

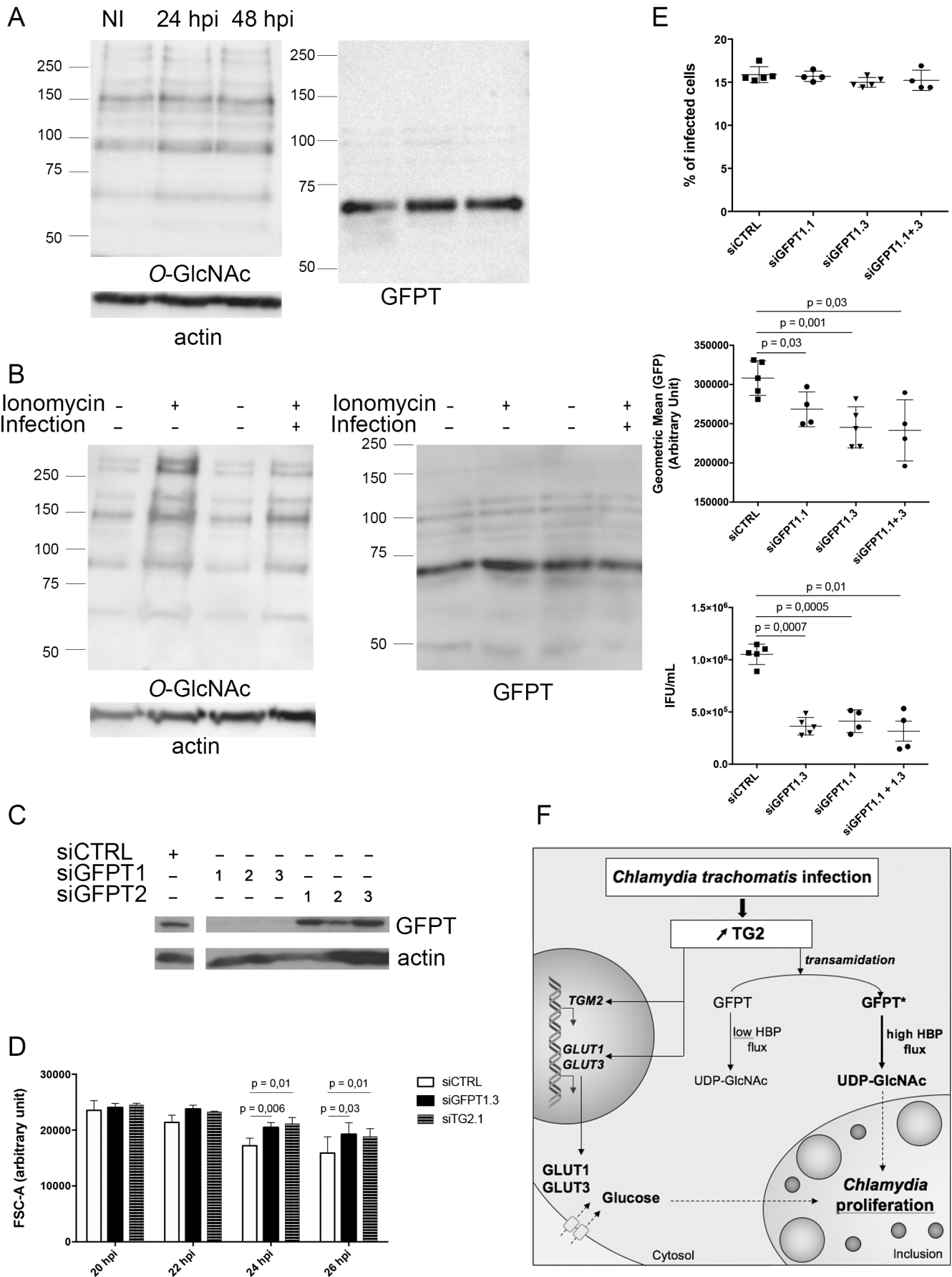
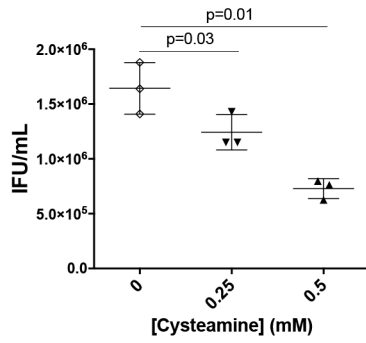
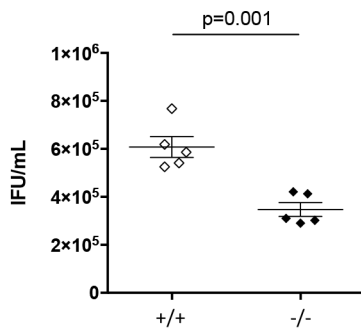


Figure EV1

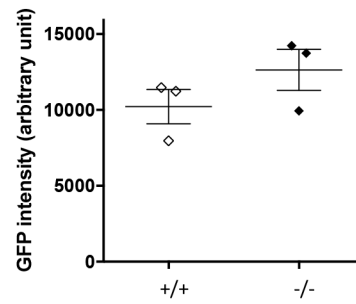
A



B



C



D

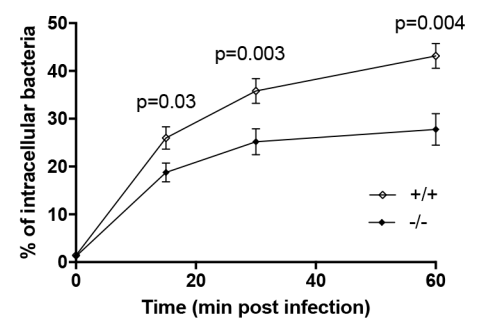
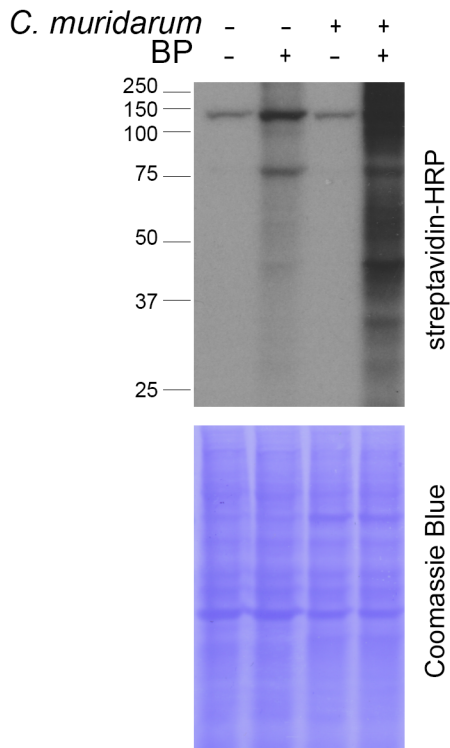


Figure EV2

A



B

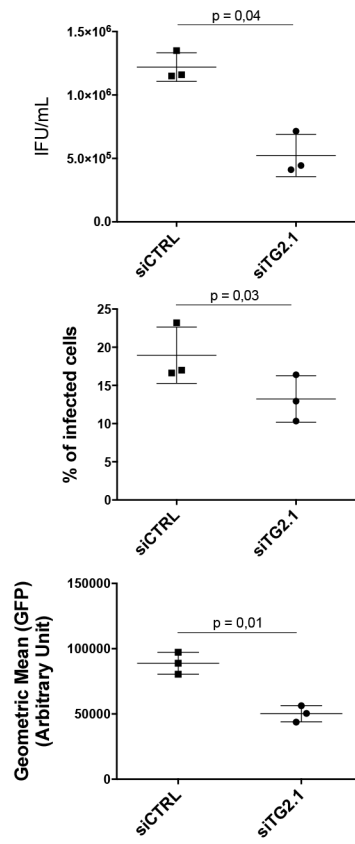
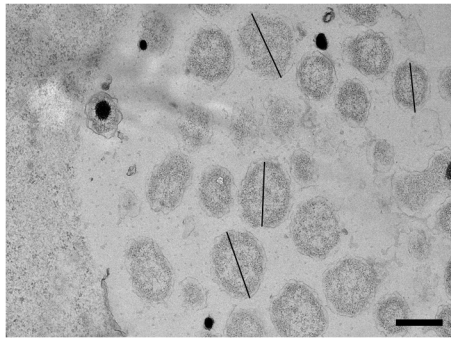
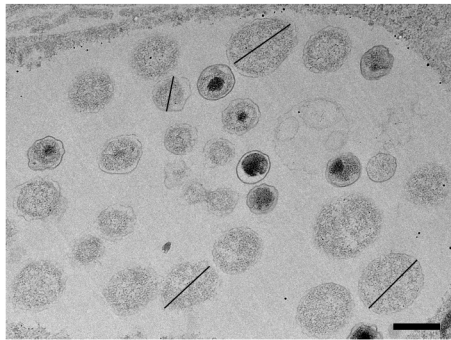




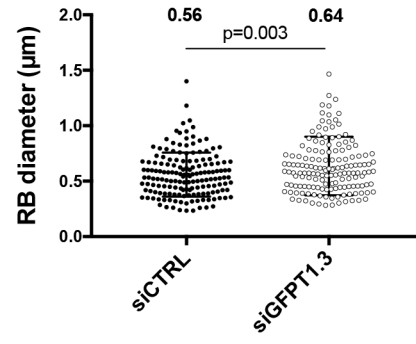
Figure EV3



siCTRL



siGFPT1



Infection-driven activation of transglutaminase 2 boosts glucose uptake and hexosamine biosynthesis

Benoit Maffei<sup>1,2</sup>, Marc Laverrière<sup>1</sup>, Yongzheng Wu<sup>1</sup>, Sébastien Triboulet<sup>1</sup>, Stéphanie Perrinet<sup>1</sup>, Magalie Duchateau<sup>3</sup>, Mariette Matondo<sup>3</sup>, Robert L. Hollis<sup>4</sup>, Charlie Gourley<sup>4</sup>, Jan Rupp<sup>5</sup>, Jeffrey W. Keillor<sup>6</sup> and Agathe Subtil<sup>1\*</sup>

## APPENDIX

### Table of contents:

- Legends to the supplementary figures
- Figure S1. **Live bacteria induce TG2 activation in HeLa and MEFs cells.**
- Figure S2. **Reduction of bacterial load does not account for the loss of induction of *GLUT-1* and *GLUT-3* transcription upon CP4d treatment.**
- Figure S3. **Measure of glucosamine-6-P production by GFPT by HPAEC-PAD.**
- Figure S4. **Gating steps for the examination of the size of replicative *C. trachomatis* by flow cytometry.**
- Table S1. **Candidate TG2 substrates in *C. trachomatis* infected cells**
- Table S2. **Primers used for siRNA, qPCR and mutagenesis**

## Legends

Figure S1. **Live bacteria induce TG2 activation in HeLa and MEFs cells.** Related to Figure 1. Before addition to HeLa cells the bacterial inoculum was either left untreated (MOI = 1), or filtered through of a 0.22  $\mu\text{M}$  filter, or incubated for 30 min at 65 °C to kill the bacteria. The inoculum was applied to HeLa cells in the presence or not of BP and 48 h later whole cell lysates were prepared. After separation by SDS-PAGE, proteins were transferred to a membrane and BP incorporation was revealed with HRP-conjugated streptavidin.

Figure S2. **Reduction of bacterial load does not account for the loss of induction of *GLUT-1* and *GLUT-3* transcription upon CP4d treatment.** Related to Figure 3. HeLa cells were infected or not with *C. trachomatis* (MOI=1) in duplicate per condition. Two hpi CP4d (40  $\mu\text{M}$ ) or 24 hpi doxycycline (62.5  $\text{ng}\cdot\text{mL}^{-1}$ ) were added to the culture medium. Forty-eight hpi DNA were extracted from one well to measure bacterial load, and RNA were extracted from the duplicate well. Bacterial gDNA (16S RNA) measured by real-time RT-PCR was normalized to host gDNA (*actin* gene) and is expressed relative to the infected non-treated culture. *GLUT-1* and *GLUT-3* transcripts were measured by real-time RT-PCR and normalized to *actin* with the  $\Delta\Delta\text{Ct}$  method as in Fig. 3A. The experiment was performed in duplicate and repeated four times, mean  $\pm$  SD are shown. P-values of the Student's ratio-paired t-test are indicated when  $<0.05$ .

Figure S3. **Measure of glucosamine-6-P production by GFPT by HPAEC-PAD.** Related to Figure 4. The three top panels show the retention times of the different sugars used or produced during the reaction when analyzed by HPAEC-PAD. Note that glutamine and glutamate are not retained by this column. A cell lysate without addition of fructose-6-P or glutamine is also shown. The bottom two panels display an enlargement of the output of the reaction when control or ionomycin treated cell lysates were used. The arrows point to the glucosamine-6-P peak. Fructose-6-P was not entirely consumed by the reaction. Formation of glucose-6-P was also observed, possibly by GFPT isomerase activity or by another cellular enzyme present in the lysate such as glucose-6-P isomerase.

Figure S4. **Gating steps for the examination of the size of replicative *C. trachomatis* by flow cytometry.** Related to Figure 6. Exponential cultures of *E. coli*, density-gradient purified elementary bodies, non-infected cells, and cells infected with L2<sup>incD</sup>GFP at MOI=0.3 for different time points (indicated) were fixed and treated as described in the methods section. The top dot plots describe how the first three samples were used to gate the region of interest that contains mostly replicative *C. trachomatis* (excluded regions are hatched). An increase in the number of replicative bacteria, and a decrease in their size (FSC-A value) were observed when increasing infection time.

Figure S1

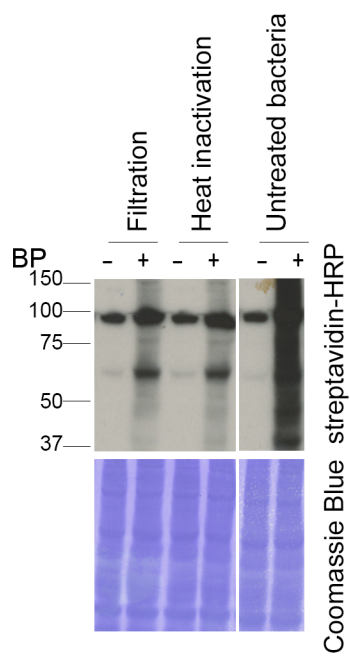


Figure S2

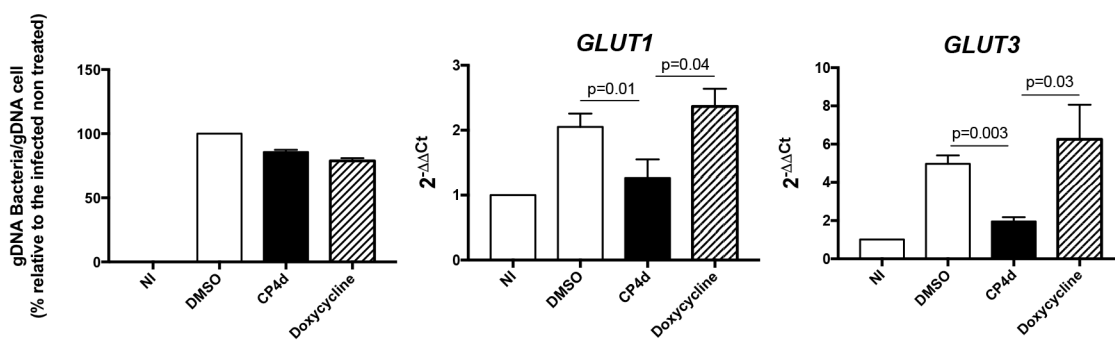
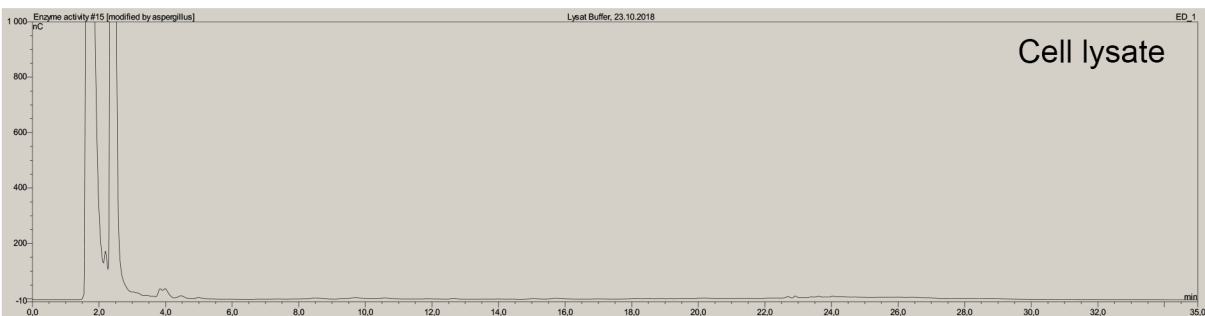
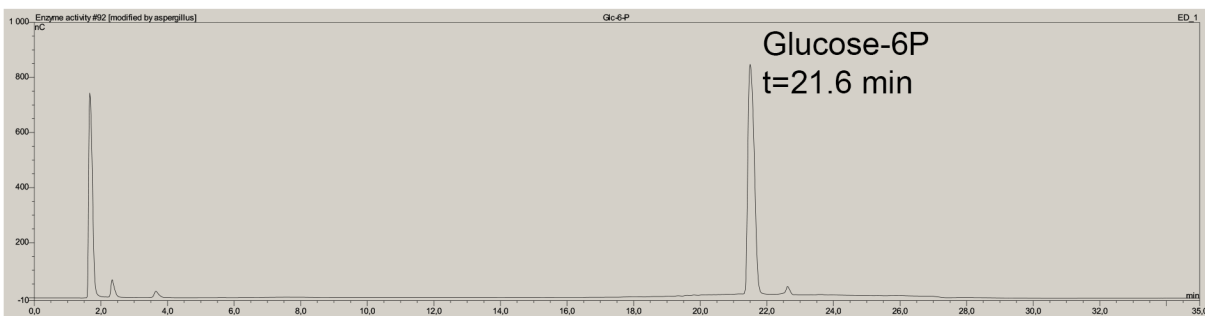
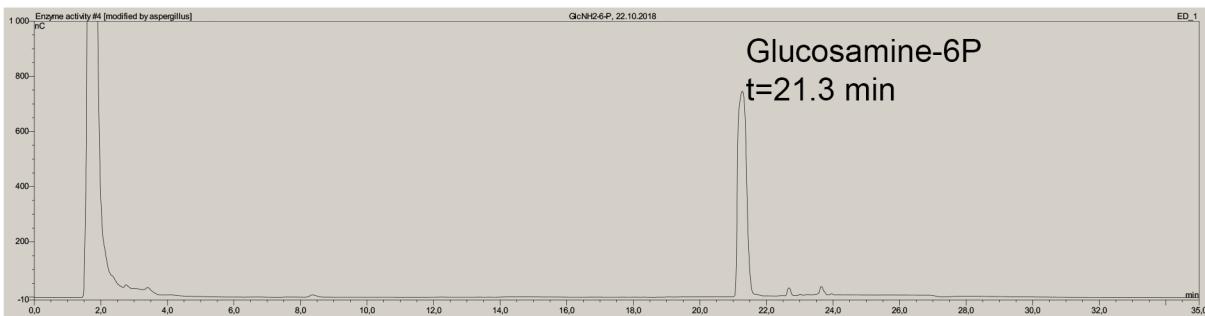
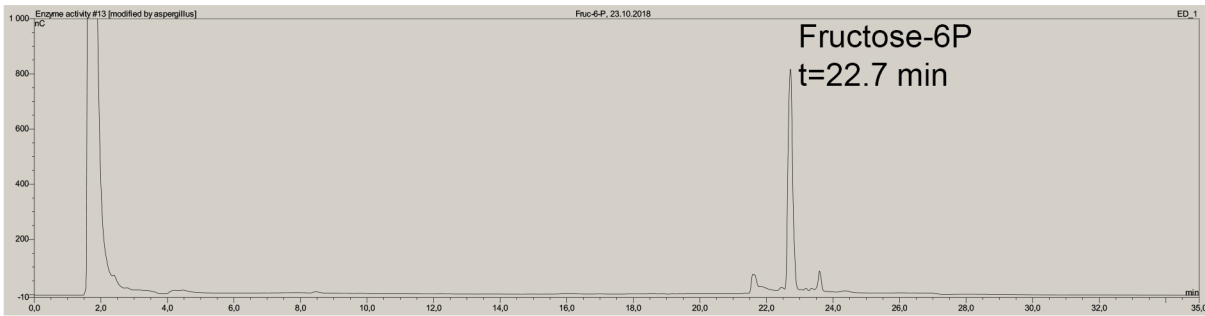
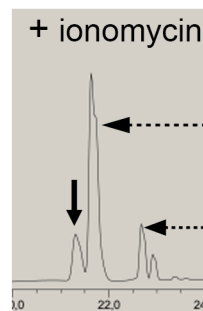
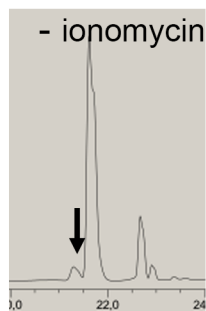


Figure S3



Reaction products:

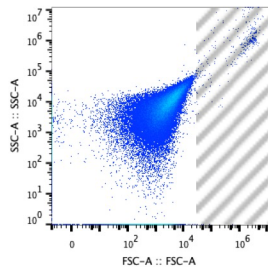


Glucose-6P

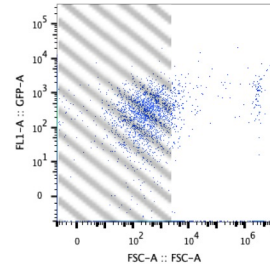
Fructose-6P

Figure S4

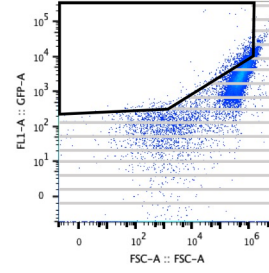
1- Gating on *E. coli*



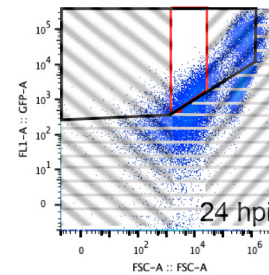
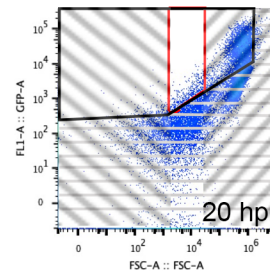
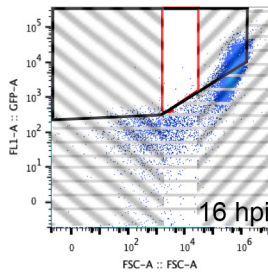
2- Exclusion of non-diving bacteria (elementary bodies)



3- Exclusion of cell debris



4 - Infected samples analysis



Infection time (h)	16	20	24
Number of events gated	53	1300	5596
FSC-A Geometric Mean	24688	18135	14445

**Table S1: Candidate TG2 substrates in *C. trachomatis* infected cells**

The list displays streptavidin-bound proteins identified by mass spectrometry in the infected samples only in the presence of BP (first 37 entries) or more abundant in the presence of BP than in its absence (last 25 entries,  $\text{Log}_2([\text{Mean intensity with BP}]/[\text{Mean intensity without BP}])$  and p-values are shown).

UniProt ID	Protein	Gene	Protein description	log2	P-value
Q8NE71-2	ABCF1	ABCF1	ATP-binding cassette sub-family F member 1	NA	NA
O95831-3	AIFM1	AIFM1	Apoptosis-inducing factor 1	NA	NA
P50995-2	ANX11	ANXA11	Annexin A11	NA	NA
P84077	ARF1	ARF1	ADP-ribosylation factor 1	NA	NA
Q13510	ASAH1	ASAH1	Acid ceramidase	NA	NA
Q12797-10	ASPH	ASPH	Aspartyl/asparaginyl beta-hydroxylase	NA	NA
P36542-2	ATPG	ATP5C1	ATP synthase subunit gamma	NA	NA
O95816	BAG2	BAG2	BAG family molecular chaperone regulator	NA	NA
Q13185	CBX3	CBX3	Chromobox protein homolog 3	NA	NA
Q9Y696	CLIC4	CLIC4	Chloride intracellular channel protein 4	NA	NA
Q16555-2	DPYL2	DPYSL2	Dihydropyrimidinase-related protein	NA	NA
P55884	EIF3B	EIF3B	Eukaryotic translation initiation factor 3 subunit B	NA	NA
P02751-4	FINC	FN1	Fibronectin	NA	NA
G3V1Q4	G3V1Q4	SEPT7	Septin 7	NA	NA
Q9HAV0	GBB4	GNB4	Guanine nucleotide-binding protein subunit beta	NA	NA
O94808	GFPT2	GFPT2	Glutamine--fructose-6-phosphate aminotransferase	NA	NA
P08754	GNAI3	GNAI3	Guanine nucleotide-binding protein G(k) subunit alpha	NA	NA
H3BSW3	H3BSW3	APRT	Adenine phosphoribosyltransferase	NA	NA
P68871	HBB	HBB	Hemoglobin subunit beta	NA	NA



A0A087WZW8	IGKV3-11	IGKV3-11	Ig kappa chain C region	NA	NA
Q15181	IPYR	PPA1	Inorganic pyrophosphatase	NA	NA
J3QLE5	J3QLE5	SNRPN	Small nuclear ribonucleoprotein-associated protein N	NA	NA
K7ENG2	K7ENG2	U2AF2	Splicing factor U2AF 65 kDa subunit	NA	NA
P17931	LEG3	LGALS3	Galectin-3	NA	NA
C9JIG9	OSR1	OSXR1	Serine/threonine-protein kinase OSR1	NA	NA
P17858	PFKAL	PFKL	ATP-dependent 6-phosphofructokinase	NA	NA
E9PQ98	PRMT1	PRMT1	Protein arginine N-methyltransferase 1	NA	NA
P62195-2	PRS8	PSMC5	26S proteasome regulatory subunit 8	NA	NA
O00487	PSDE	PSMD14	26S proteasome non-ATPase regulatory subunit	NA	NA
Q16401-2	PSMD5	PSMD5	26S proteasome non-ATPase regulatory subunit 5	NA	NA
Q06203	PUR1	PPAT	Amidophosphoribosyltransferase	NA	NA
P17812-2	PYRG1	CTPS1	CTP synthase 1	NA	NA
P43487-2	RANG	RANBP1	Ran-specific GTPase-activating protein	NA	NA
Q9P2E9-2	RRBP1	RRBP1	Ribosome-binding protein 1	NA	NA
P56192	SYMC	MARS	Methionine--tRNA ligase	NA	NA
O95497	VNN1	VNN1	Pantetheinase	NA	NA
E9PRD9	VNN2	VNN2	Vascular non-inflammatory molecule 2	NA	NA
P08243-2	ASNS	ASNS	Asparagine synthetase	7,62	1,81E-08
P30508	HLA-C	HLA-C	HLA class I histocompatibility antigen, Cw-12 alpha chain	9,05	4,07E-08
P35613-2	BASI	BSG	Basigin	2,33	1,85E-05
P10909-4	CLUS	CLU	Clusterin	2,13	3,91E-05

P49368	TCPG	CCT3	T-complex protein 1 subunit gamma	1,83	3,99E-04
O15427	MOT4	SLC16A3	Monocarboxylate transporter 4	1,93	6,21E-04
E9PLL6	RPL27A	RPL271	60S ribosomal protein L27a	1,36	9,12E-04
Q15233	NONO	NONO	Non-POU domain-containing octamer-binding protein	1,26	1,21E-03
P30837	AL1B1	ALDH1B1	Aldehyde dehydrogenase X	1,98	1,50E-03
E9PLA9	CAPRIN1	CAPRIN	Caprin-1	1,47	1,61E-03
P17987	TCPA	TCP1	T-complex protein 1 subunit alpha	1,91	2,84E-03
P39019	RS19	RPS19	40S ribosomal protein S19	1,44	3,74E-03
O43143	DHX15	DHX15	Putative pre-mRNA-splicing factor ATP-dependent RNA helicase	1,00	4,00E-03
P61586	RHOA	RHOA	Transforming protein RhoA	1,01	4,49E-03
C9J9K3	RPSA	RPSA	40S ribosomal protein SA	1,07	4,91E-03
A0A087WXM6	RPL17	RPL17	60S ribosomal protein L17	1,01	5,48E-03
P38919	EIF4A3	EIF4A3	Eukaryotic initiation factor 4A-III	1,08	7,23E-03
P00505	AATM	GOT2	Aspartate aminotransferase, mitochondrial	1,11	8,63E-03
P27105	STOM	STOM	Erythrocyte band 7 integral membrane protein	1,01	9,61E-03
A0A096LNZ9	ISG15	ISG15	Ubiquitin-like protein ISG15	1,25	1,10E-02
E9PEX6	DLD	DLD	Dihydrolipoyl dehydrogenase, mitochondrial	1,08	1,66E-02
Q10589-2	BST2	BST2	Bone marrow stromal antigen 2	1,15	2,37E-02
Q06210	GFPT1	GFPT1	Glutamine--fructose-6-phosphate aminotransferase	3,22	2,49E-02
A0A087WVM3	CYR61	CYR61	Protein CYR61	1,34	2,75E-02
Q13162	PRDX4	PRDX4	Peroxiredoxin-4	1,13	2,88E-02

**Table S2: Primer sequences used for siRNA, qPCR and mutagenesis**

Experiment	Target	Sequence
siRNA	TG2.1	GGGCGAACCACCUGAACAAAdTdT
	TG2.2	CAGUUCGAGGAUGGAAUCCUGGAUAdTdT
	HIF1 $\alpha$ .1	AAGUCUGCAACAUGGAAGGUAdTdT
	HIF1 $\alpha$ .2	UUCUCCGAACGUGUCACGUdTdT
	GFPT1.1	GACAGAUUGUGGAGUUCAUdTdT
	GFPT1.2	CCUUGGUGGAGAGAGUUAUdTdT
	GFPT1.3	GUGACUCCUGGACAGAAAdTdT
	GFPT2.1	GUUCCAAGUUUGCGUAUAAAdTdT
	GFPT2.2	GACCGAAUUUCACUACAAAdTdT
	GFPT2.3	CCAUCGCCAAGCUGAUUAAdTdT
qPCR	$\alpha$ -actin	GGACTTCGAGCAAGAGATGG
		GCAGTGATCTCCTTCTGCATC
	<i>Chlamydia</i> 16S RNA	TGGATGAGGCATGCAAGTA
		TACTAACCCCTCCGCCACTAAA
	Mouse 18S RNA	TAACGAACGAGACTCTGGCAT
		CGGACATCTAAGGGCATCACAG
	TG2	TAAGAGATGCTGTGGAGGAG
		CGAGCCCTGGTAGATAAA
	GLUT-1	AACTCTCAGCCAGGGTCCAC
		CACAGTGAAGATGATGAAGAC
	GLUT-3	CACAGGTTTTGTGCCATGTA
		ACCCCGCAGGGCAGTAG
Mutagenesis	Q58N	GGGAAGCCAATGCCTGCAAAATCAATCTTATTAAGAAGAAAGGAAAAGT
		ACTTTTCCTTCTCTTAATAAGTTGATTTGCAGGCATTGGCTTCCC
	Q326N	CGAGCTGTGCAAACACTCAATATGGAAGTCCAGCAGATC
		GATCTGCTGGAGTTCATATTGAGTGTTTGCACAGCTCG
	Q548N	CGAAATTCAGAACTAGCAACAGAACTTTATCATAATAAGTCAGTTCTGATAATG
		CATTATCAGAACTGACTTATTATGATAAAGTTCTGTTGCTAGTTTCTGAATTCG